CPRC
CANADIAN POLICE RESEARCH CENTRE

CCRP
CENTRE CANADIEN DE RECHERCHES POLICIÈRES

TR-03-91
Feasibility Study of a Laser Traffic Radar

André Morin, Yves Taillon, Sylvain Lord and Alain Mailloux
National Optics Institute

TECHNICAL REPORT

August 1991

NOTE: Further information about this report can be obtained by calling the CPRC information number (613) 998-6342

FINAL REPORT

FEASIBILITY STUDY OF A LASER TRAFFIC RADAR: A PROOF OF CONCEPT

INO 91-5306PC RFI N/A

Work performed under contract
#31947-0-0003/01-SS

Submitted

to

John G. Arnold

Canadian Police Research Center
National Research Council of Canada
Institute for Information Technology
Montreal Road Labs, Building M-50
Ottawa, Ontario, K1A 0R6

by

André Morin
Yves Taillon
Sylvain Lord
Alain Mailloux

National Optics Institute
369 Franquet, Ste-Foy
Québec, G1P 4N8

AUGUST 1991

SUMMARY

This report describes and presents results obtained with a laser based traffic radar prototype. The technique used in the laser radar prototype is the time of flight. It was chosen after the theoretical feasibility study performed during the first part of the contract. The laboratory prototype mainly comprises two parts; an optical system and a signal processing unit.

Different car paints and parts are analysed. After different tests comprising field tests it is shown that the laser echo from the radar is more likely to come back from an headlight or front license for an incoming car and from retroreflectors incorporated in rear parking lights for a receding car.

It is shown that the collimator of the radar laser diode gives best results when it is made of both a spherical and a cylindrical lens. For the receiving lens, a lens of Fresnel type gives better results than a glass lens. The noise background signal is also observed to decrease by a factor of 4 and the signal by a factor of 2 when using a laser line filter in front of the detector. Then, this increases the signal-to-noise ratio by a factor of 2.

Field tests on moving cars are briefly described. An aiming system mounted on the radar prototype greatly facilitates the tracking of the cars. A riflescope is used as the aiming system in the present case.

The best ranges obtained with the optical system and an oscilloscope, e.g. the maximum ranges at which the return signal is still distinguished on the oscilloscope screen are respectively 700 m for an incoming car and 1200 m for a receding one. The humidity and dust content of the air, as well as the noise induced by sun light are all decreasing the maximum range. With a high degree of humidity, a strong wind (dust in the air) and at noon, the maximum attainable ranges are decreased by a 20% factor compared to the maximum ranges.

Using the complete system, e.g. the optimized optical system with the signal processing unit, the maximum ranges are respectively decreased to 400 m and to 600 m for an incoming and a receding car. The incertitude given by the confidence interval, σ, on the speed measurement distribution is 3.7 km/h. This incertitude is believed to mainly come from the long laser pulsewidth (200 ns), it is the belief of the authors that this incertitude can be decreased to a much lower value.

Two different design proposals for an industrial prototype are also presented and described. The final design will have to be chosen after discussion with the producer company and the police community.

Table of Contents

List of Figures and Tables

1. INTRODUCTION.

A laser based traffic radar is a system expected to offer many advantages over a conventional microwave radar. For example, conventional radars are often difficult to operate, being prone to parasitic radio sources, as well as unwanted reflections and interferences. In contrast, the light beam emitted by the laser based device would be immune to such influences. Since the laser provides a very narrow beam (contrary to typical emission lobes of X/K-band radars), the laser radar has excellent directionality, permitting selective measurement on one vehicle even in high density traffic. As a second consequence, the laser-based radar would render obsolete the actual radar detectors and would discourage the use of such devices. It is also felt that efficient counter-measure systems would be extremely difficult to develop.

This report presents the final results and conclusions related to the feasibility study of a laser traffic radar. The work has been performed under contract 31947-0-0003/01-SS from Supply and Services Canada. It was divided into two main parts: a theoretical feasibility study and the realization of a laboratory prototype laser traffic radar. The theoretical report has been submitted at the beginning of last April to Mr. John G. Arnold from CPRC [1].

In the theoretical report, three different techniques of speed measurements were evaluated. From a complexity and cost point of view, two techniques which used an energy detection were identified as the most promising. When comparing these two techniques, the time of flight and the phase modulation, the first one appeared to be somewhat less precise but appeared also to be less sensitive to noise and atmospheric conditions. We then choose to build a laboratory prototype using the time of flight technology for the second part of the feasibility study. Would there be a very reliable modulated laser diodes in the 50-500 MHz range at an acceptable cost, the phase modulation technique would have to be considered back. From now on, we will concentrate on the laboratory prototype using the time of flight technology and references to the theoretical report will be made when necessary.

Since the laboratory prototype comprises two different sub-systems, an optical unit and a data processing unit, the report will be divided in two main parts. Sections 2, 3 and 4 will cover the optical part where the optical behaviour of different parts of a car, the description of the optical components of the laser traffic radar and the field test results will respectively be presented. In the other part, Sections 5 through 8 will concentrate on the signal processing. Section 5 will briefly review the conclusion and recall the main equations of the interim report. Section 6 will present the block diagrams of the processing circuit while section 7 will present the field test results. Section 8 will present some improvements that should be implemented in the final design, and finally, section 9 will be devoted to the discussion of the results and to the proposal of an industrial prototype. A brief conclusion will follow.

Note: The reader who does not want to read the entire report may concentrate on the conclusion of section 3, and on sections 4, 8 and 9.

2. OPTICAL CHARACTERISTICS OF A CAR.

The laser traffic radar being based on the echo analysis of an optical signal reflected from a moving car, it is very important to know the optical properties of different parts of a car. In section 2.1, we will first present a spectrometric analysis of different car paints, e.g. different colors and their reflective properties. Then, we will present in section 2.2 a field test like comparative study of many components of a car (paints, headlights, etc.). This comparison will be made with a laser diode emitting at a fixed wavelength and the receiver will be set in a geometry similar of the one used in the laser traffic prototype. Section 2.3 will give a brief conclusion.

2.1 SPECTROMETRIC ANALYSIS OF CAR PAINTS.

2.1.1 Physical definitions.

When light impinges onto a surface of any kind of material, it undergoes one or more of the following phenomena: a reflection, a refraction, an absorption or a diffusion. This section presents a spectrometric analysis of the reflectance characteristics of different car paints deposited on aluminium surfaces (by reflectance, we mean both specular and diffuse).

A specular reflection occurs whenever the light energy travels in a definite direction after having hit the reflecting surface. Moreover, in the case of a specular reflection the image of the original source can be seen by an observer placed at a right position. The reflecting surface then appears to be an aperture through which the source is seen. This kind of reflection happens when the encountered surface is very well polished (e.g. the surface is very smooth). When the surface is not smooth, every irregularity of the surface will reflect the light in a different direction, and the light will not return to the observer as a definite beam. It is then a diffuse reflection and the surface itself will be visible from all directions. The light may be considered as spreading out from every point on the surface (all illuminated objects are visible by reason of the light irregularly reflected at their surfaces).

To measure the diffuse reflectance we need to use an integrating sphere. This kind of sphere integrates the diffuse signal over a 2 π steradian solid angle. At a certain distance of a target the focussing lens of the system will only collect a small amount of the diffuse signal since this diffuse signal is spread over an hemisphere. Figure 2.1 shows the diffusion spreading of an ideal Lambertian body and figure 2.2, the integrating sphere measurement set-up (a Lambertian surface is defined as a surface from which the luminous flux reflected per unit solid angle is proportional to the cosine of the angle measured from the normal to the surface).

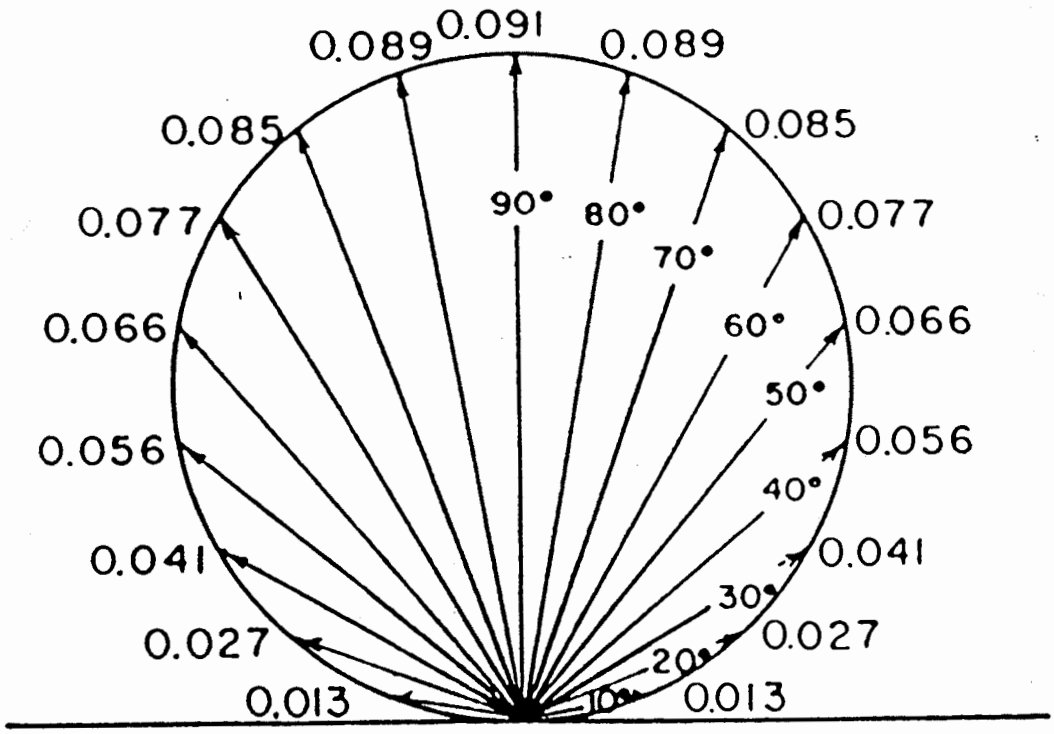

Figure 2.1 Intensity distribution of light reflected from a perfectly diffuse (Lambertian) surface, showing proportion of reflected light within 5° of each indicated direction [from ref. 2].

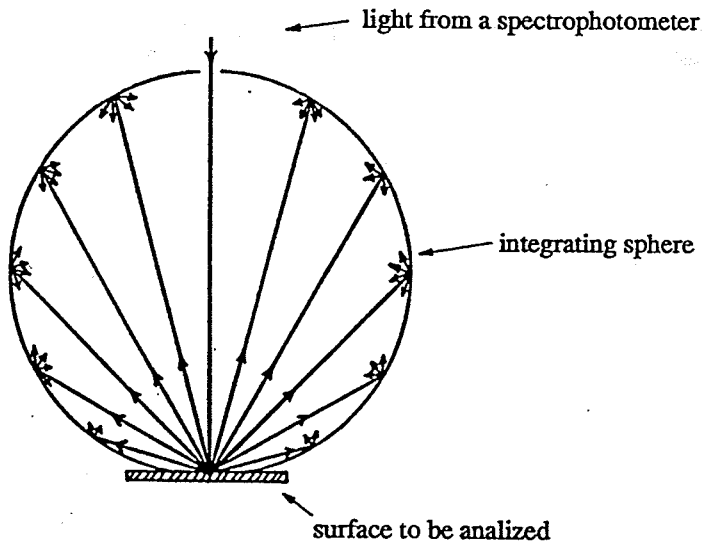

Figure 2.2 Integrating sphere measurement set-up for total diffuse reflectance [from ref. 3].

2.1.2 Spectrometric analysis.

The spectral range covered by the spectrometer varies from 600 nm to 950 nm. To cover the range, two different lamps are used in the spectrometer. One covers the 600 nm to 800 nm range and the other, the 800 nm to 950 nm range. We analyzed seven different colors. Figure 2.3 presents the percentage of specular reflection of each paint. From this figure, it is seen that the specular reflectance is roughly the same for every color. The mean value can be evaluated to be around 4 %. Since there is a lot of noise from 800 nm to 950 nm, it is difficult to estimate if the specular reflectance varies for different colors in that region. From the tests presented in section 2.2, we will be able to see if there are such variations at least at the 860 nm wavelength.

Figure 2.4 presents the diffuse reflectance of the 7 paints. The diffuse reflectance varies greatly from one paint to the other. It is less than 5 % for 4 of the paints, namely for black metallic, black, blue metallic and blue paints and goes up to 75 % for the white while brown and red give respectively 10 % and 45 %. The method used to measure the diffuse reflectance suggests that the diffusion will be of greater imporantce than the specular reflections to send back the laser echo. It will be seen that this will not necessarily be the case since the diffuse reflectance has been measured with an integrating sphere.

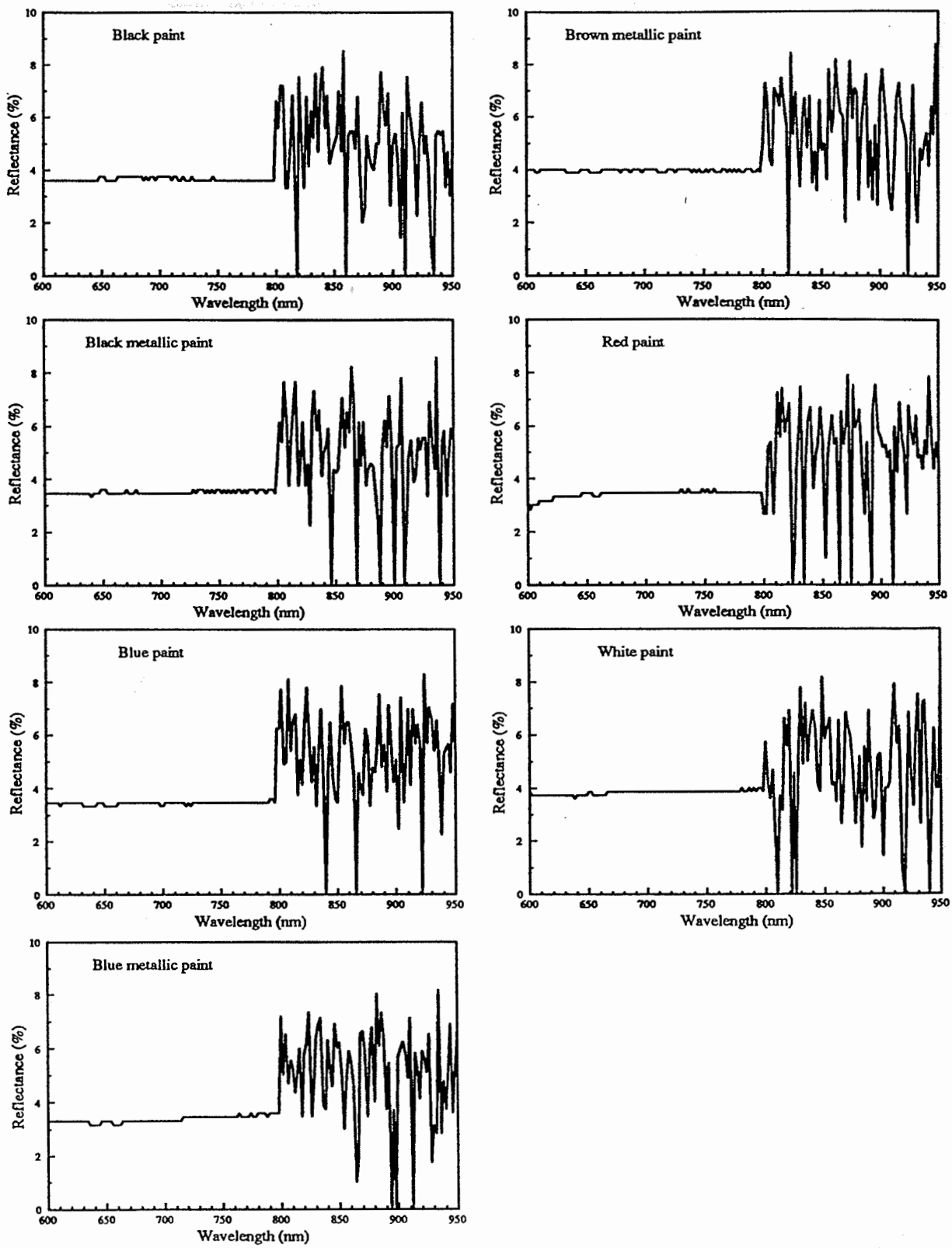

Figure 2.3 Specular reflectance versus wavelength for different paint colors.

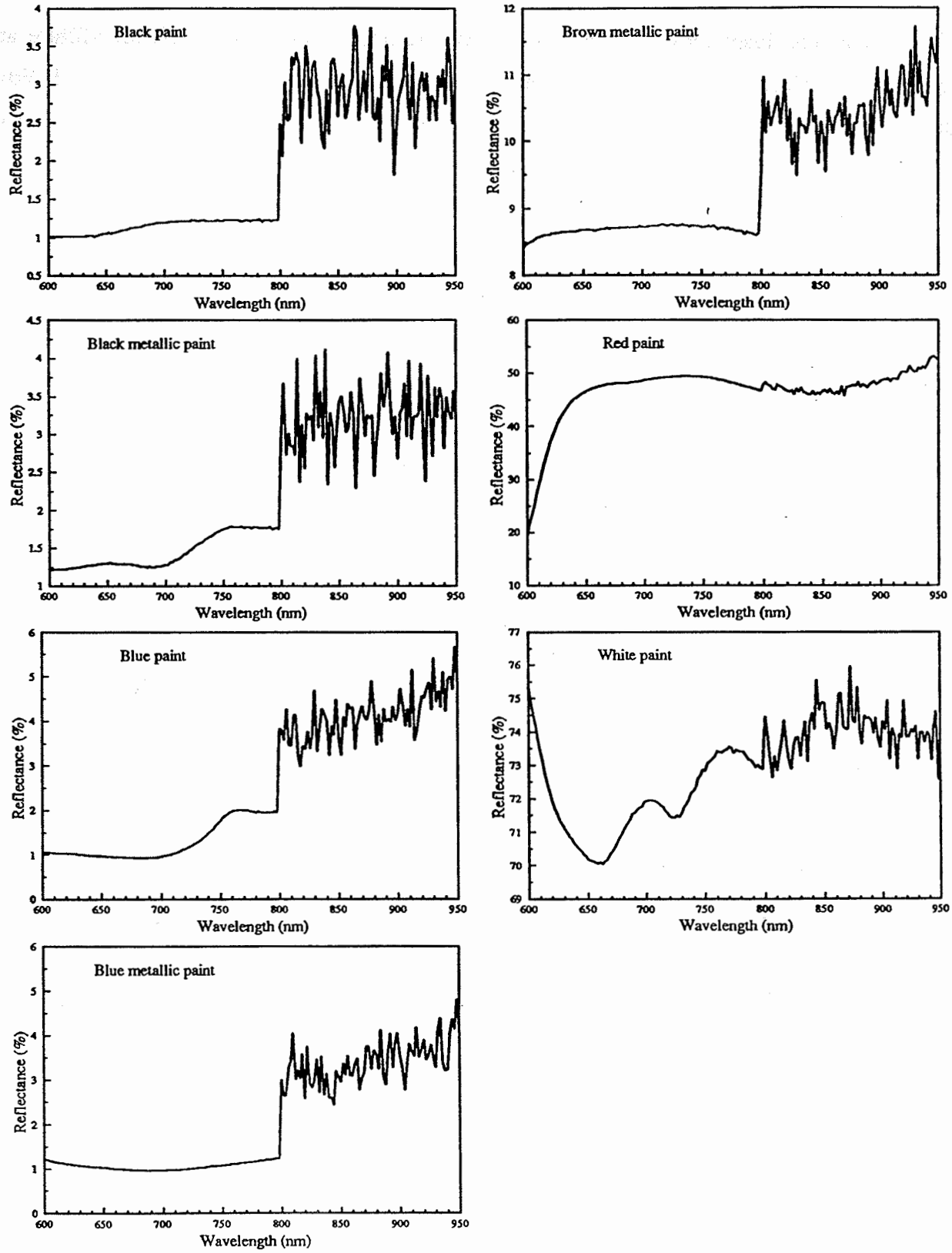

Figure 2.4 Diffuse reflectance versus wavelength for different paint colors.

It is also interesting to note that neither one nor the other paint reflects (diffuse and specular) 100 % of the light. Then the part of the light which is not reflected is absorbed. From figures 2.3 and 2.4, one can see that, as expected in this part of the electromagnetic spectrum, black and blue paints are the most absorbing while red and white paints are the most reflecting.

2.2 REFLECTIONS MEASURED WITH A RADAR-LIKE SET-UP.

As mentioned earlier, the measurements taken with an integrating sphere could be misleading in the evaluation of the most effective part of a car to return the laser echo. A verification of this statement was made using a set-up very similar to that of the police radar and measured the specular and diffuse reflectances of different car parts. Figure 2.5 shows the measurement set-up, where the emitter is a 860 nm laser diode (CVD-97 from Laser Diode Inc.). The detector used was a radiometer with a 1 cm diameter surface. With a solid angle corresponding to that aperture (lenses were not used), we measured the mean signal. The different targets were placed at a distance of 9.1 meters (30 feet) from both the laser and the receiver.

Figure 2.6 shows the measured reflectances, specular (light part) and diffuse (dark part), for the 7 car paints. The diffuse reflectances on that figure were taken when the painted plates made an angle of about 5° with the laser beam direction. Figure 2.7 shows the reflectances of different car parts like headlight, tire, etc. Each measure of figure 2.6 and 2.7 is normalized to the specular reflectance of white paint and the reflectance is given on a logarithmic scale. From figure 2.6, it is seen that the specular reflectance is greater than the diffuse reflectance for all the paints and that by at least a factor of 15. This factor will increase with the range of the target.

Hence, the echo from the body of the car will be much more important if the measured signal comes back after a specular reflection. This statement implies that a car will be much more easy to see with the radar if a part of it is aligned in such a way that the light emitted by the laser radar is directly returned back to the radar after reflection. It is then very easy to imagine that some kind of cars will be more difficult to see from the paint because of their color

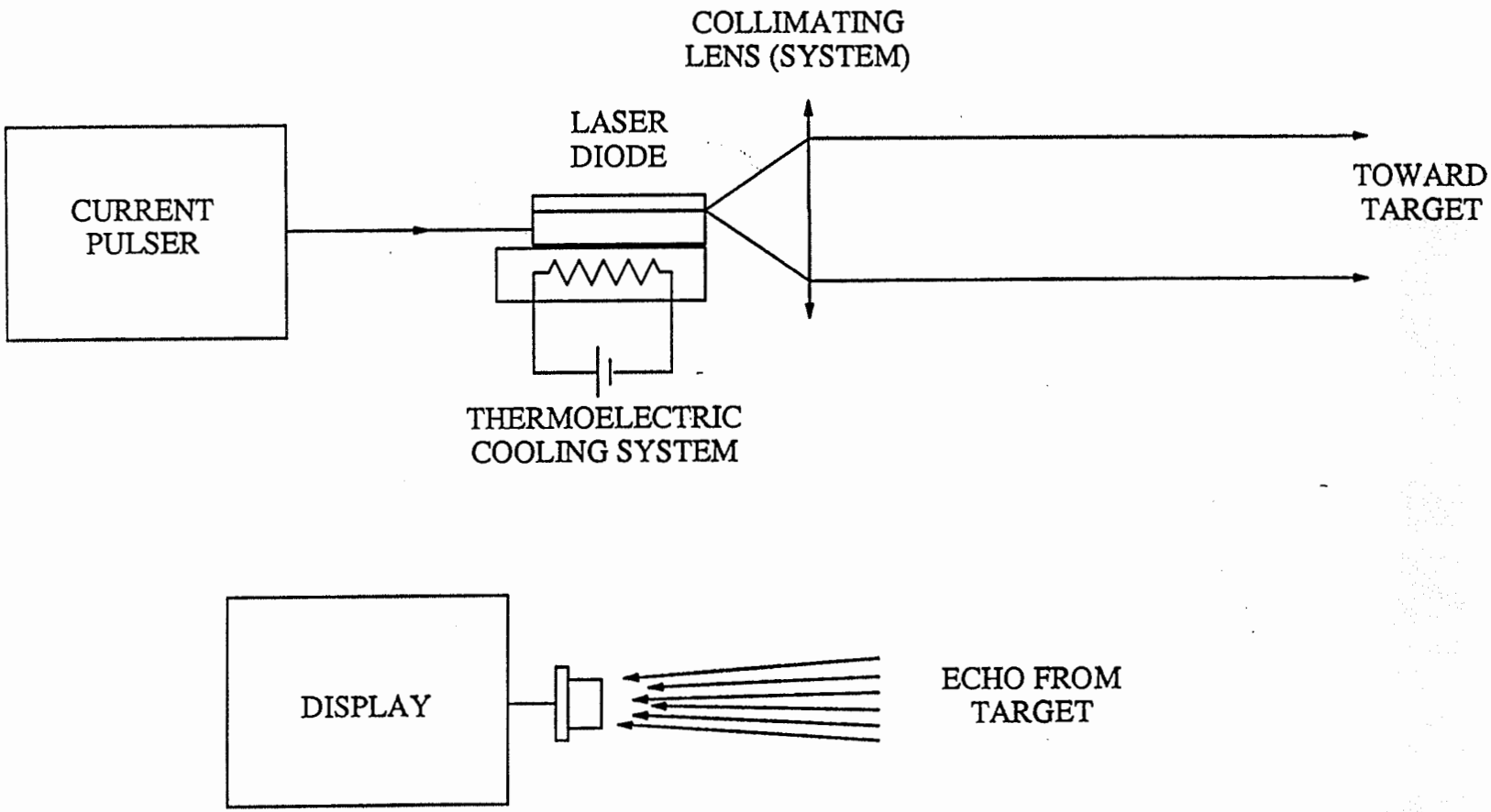

Figure 2.5 Radar-like measurement set-up for reflectances (diffuse and specular).

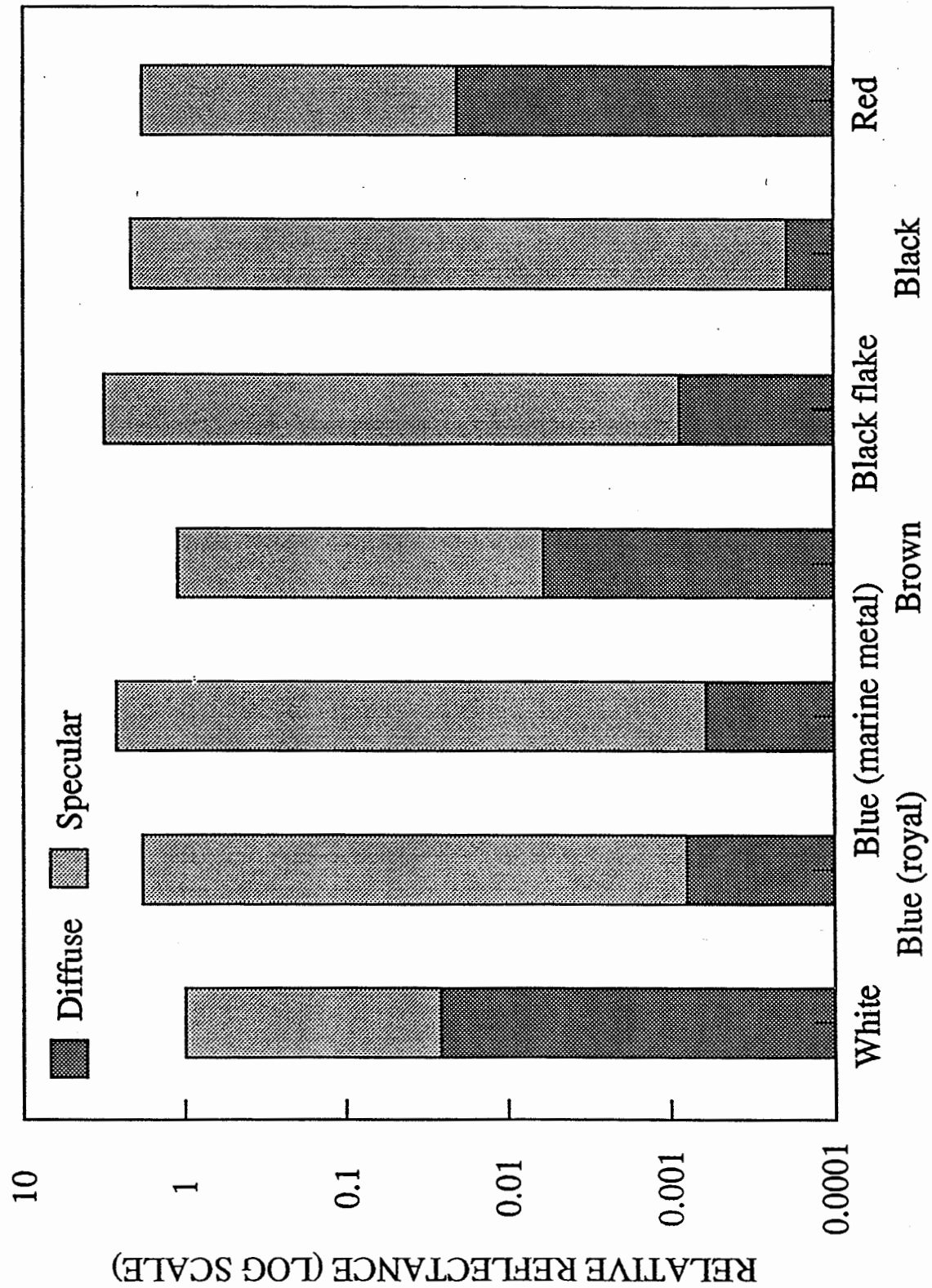

Figure 2.6 Relative specular and diffuse reflectances of different car paints.

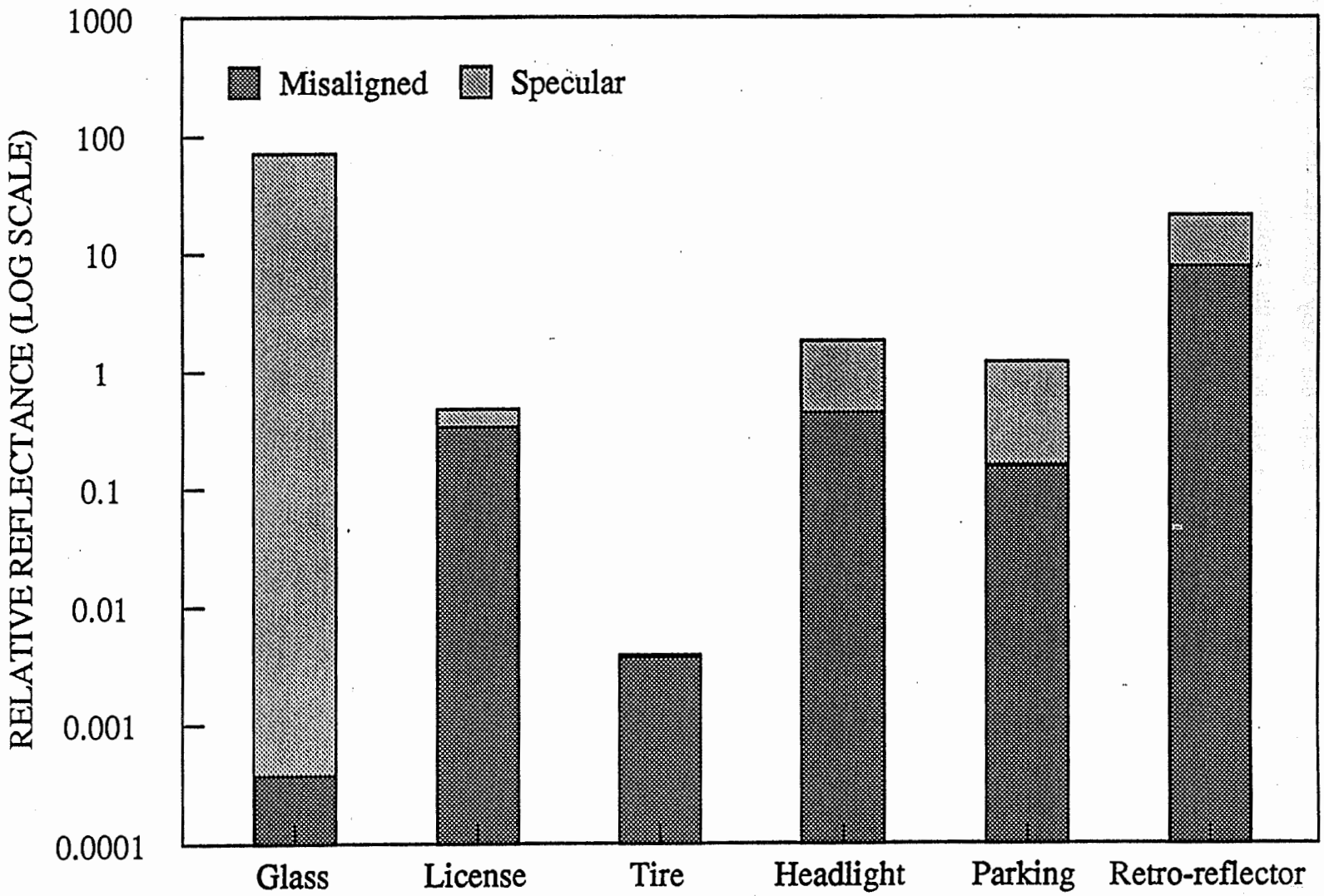

Figure 2.7 Relative specular and diffuse reflectances of different car parts.

and mostly because of their shape in the case where the body does not have any surface perpendicular (aligned) to the radar. However, we will see that this problem will be overcome by the constant presence on car of some parts that are particularly efficient in returning the impinging light.

On figure 2.7, we can see the reflectances (specular and diffuse) of many other car parts. Since the glass (windshield) is a very well polished surface, the specular reflectance is very high and the diffuse reflectance, very low. Unfortunately, the windshield is always inclinated with respect to the horizontal and the specular reflection is more likely to be directed somewhere else than back onto the radar.

The license shows a particularly high diffuse reflectance which is almost as high as the specular one. This is due to the fact that licenses are painted with special diffusing paints. Therefore, in provinces and countries where front and back licenses are both used, this will be a very good target to aim at.

On figure 2.7 we also see that the tire reflectance is very low. We can then be sure that no special signal modification will be encountered due to tires rotation that might induce erroneous signals.

A headlight was also analysed. The two reflectances shown on the histogram are, in that case, specular reflections. One stands for a very well aligned headlight (highest signal) and the other, for a misaligned one. Even when the headlight is not aligned, the echo signal is still very high. Moreover, since more and more cars are now moving with headlights on even in daylight, the headlights are very good targets to aim at, especially where front licenses are not used.

In the back of a car, the license will always be a good target. Also, every car have parking lights in their back. These parking lights are quite good reflectors even when misaligned as can be seen from figure 2.7. Moreover, in each parking light there is a retroreflector surface which is made of corner cubes. These corner cubes have the ability to return light directly to

the point where it is emitted no matter of the incoming direction. Then, a corner cube surface never needs to be aligned and always shows specular reflection. Figure 2.7 shows the signal level when the retroreflector is almost perpendicular to the radar beam (highest signal) and when the normal to the retroreflector surface makes an angle of 20° with the direction of the radar beam. It is seen from figure 2.7 that retroreflector surfaces are ideal targets to aim at when very long ranges are needed. Unfortunately, there are no such retroreflecting surfaces in front of a car.

2.3 DISCUSSION.

From figures 2.6 and 2.7, it is clear that the echo needed to measure a car speed is most likely to come back from the license, or the headlight when measuring an incoming car, and from the license or the retroreflector surfaces in the parking lights when measuring a car that goes away. In the field tests section, we will see the performances of the laser based traffic radar when aiming at headlights or retroreflectors.

3. LASER RADAR SET-UP DESCRIPTION.

This section will describe the optical components and characteristics of the laser traffic radar prototype. Since the optical system is divided into two parts, the description will also be divided into 2 parts: the optical emitter (section 3.1) and the optical receiver (section 3.2). The optical experimental set-up is shown on figure 3.1.

3.1 THE EMITTER.

3.1.1 Measurement method.

We must now recall the basic principles of the measurement method used, the time of flight. With this method we simply measure the range of a car at two different moments and then divide the travelled distance by the time interval between the two measurements to obtain the speed. Figure 3.2 illustrates the method. The range is deduced from the time of flight taken by a pulse of ligth to cover the distance to the car and to come back.

3.1.2 Emitter characteristics.

The basic part of the emitter is the laser diode. As can be seen from figure 3.1, this laser diode is mounted on a thermoelectric cooler. This cooling component is not mandatory in the system but it helps protecting the laser diode against overheating.

The laser diode is a CVD-97 from Laser Diode Inc. It works only in pulsed mode and the duty factor is 0.1 %. The wavelength at 25°C is 860 nm. To obtain very good results with the time of flight technique, we need a very good current pulser to drive the laser diode. This means that the pulser has to supply a very high current pulse in a very short time at a very high repetition rate (see preliminary report for requirement details [1]). The current pulser that we had (IL20C from Power Technology Inc.) gave a maximum current of 25 A in a 200 ns pulsewidth. The temporal pulse shape is shown on figure 3.3.

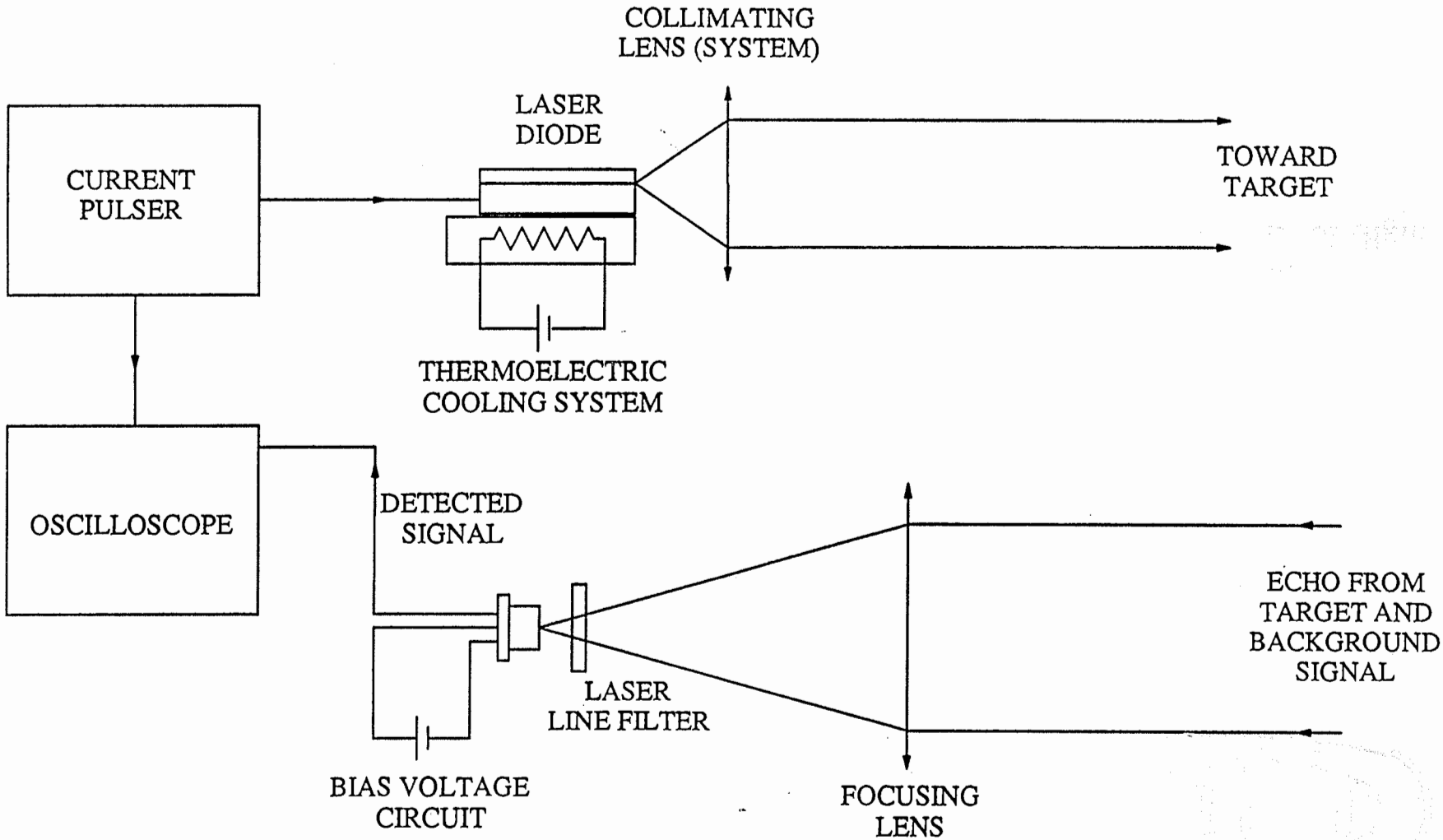

Figure 3.1 Laser traffic radar optical set-up.

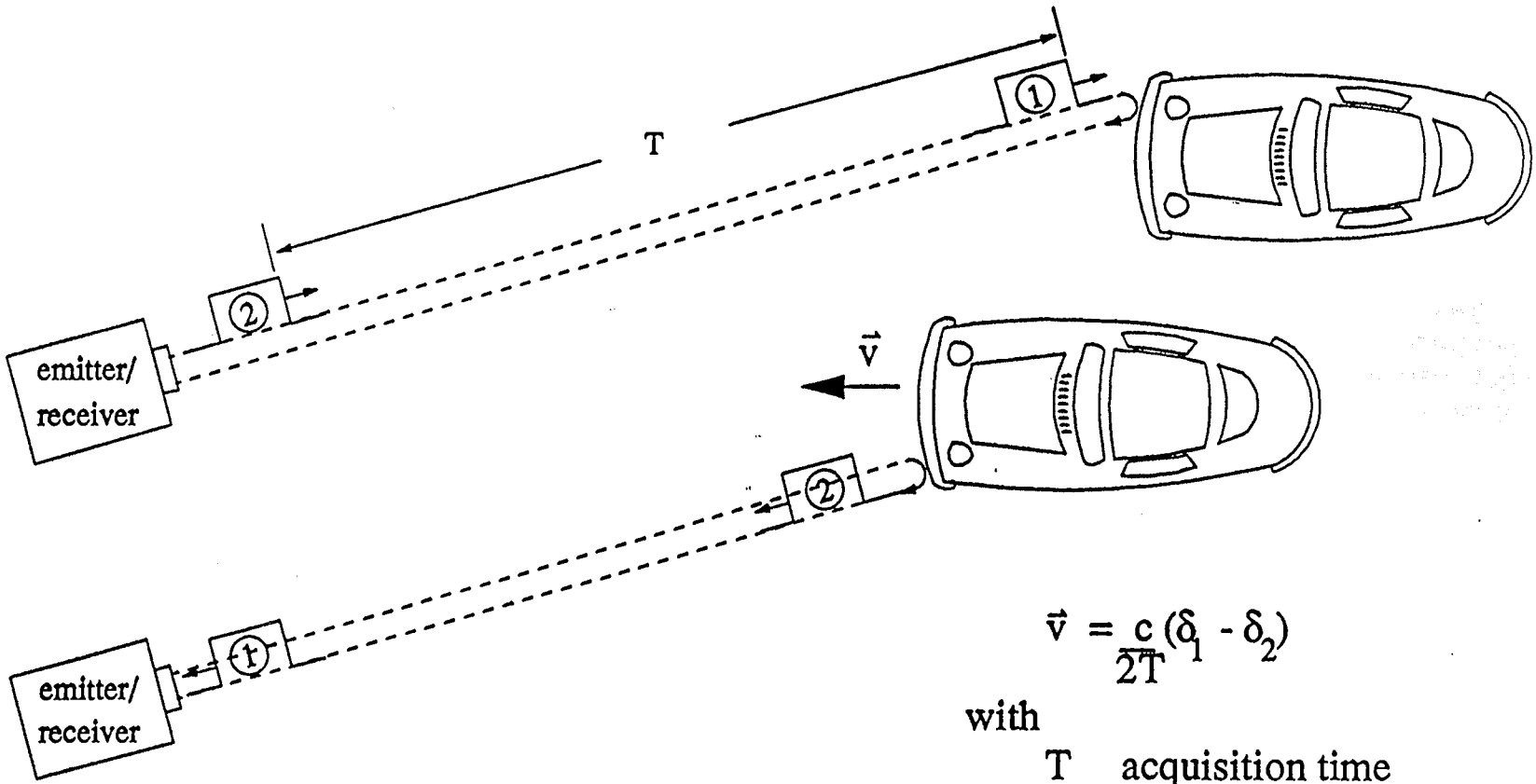

Figure 3.2 The time of flight (TOF) technique.

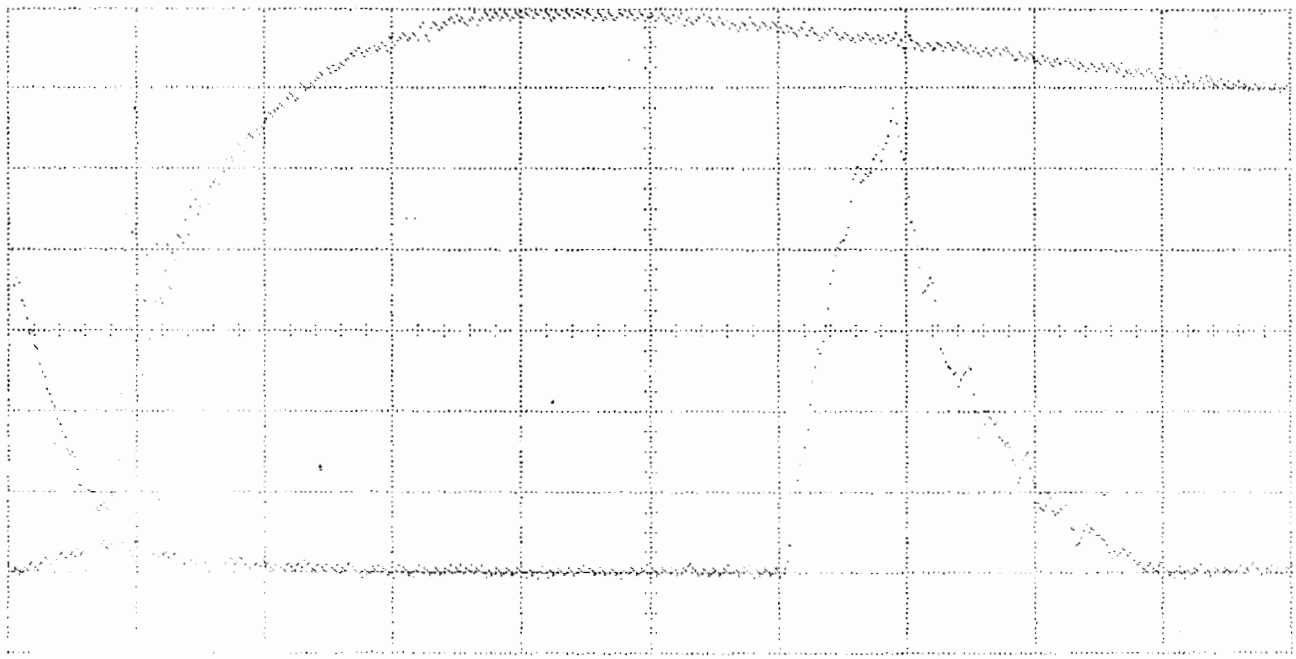

Ch. 1 = 50.00 mVolts/div
Ch. 2 = 100.0 mVolts/div
Timebase = 100 ns/div

Figure 3.3 Laser diode emitted pulse shape.

Laser diodes have some characteristics that we have to deal with. One of those is the beam divergence which is very large and not equal in the parallel and perpendicular planes of the junction. Figure 3.4 a) and b) show respectively the beam spread in the planes normal and parallel to the junction. The divergence of a laser diode beam being very large (more than 30° on one axis), we need to collimate its output light. The collimating system can be a simple spherical lens or can be made of a set of spherical and cylindrical lenses.

There is always a limit to which we can correct the divergence of a light source. This limit depends on the size and shape of the source. The diverging angle of the beam after collimating, θ, is related to the size of the source and the focal length of the focussing lens as follow:

$$\tan \frac{\theta}{2} = \frac{D}{2f} \quad , \tag{3.1}$$

$$\theta \approx \frac{D}{f} \ (\textit{for small angles}) \quad , \tag{3.2}$$

where θ is the diverging full angle in one plane, D is the height of the source in that plane and f, the focal length of the collimating lens. In our case, the laser diode stripe is 380 μm x 2.0 μm. We then see from equation 3.2 that the output light from our laser diode will diverge at a greater rate in the normal-plane than in the parallel-plane when using only spherical lenses. That is why cylindrical lenses are often used along with spherical lenses to collimate laser diodes. They allow the light to be collimated in one plane at a time with lenses of different focal powers and then the divergence can be made equal in both planes.

Three different collimating systems will be compared in chapter 4 during field tests. Field tests are needed to choose the most effective collimating system since we do not know exactly the contribution of each part of the car to return the signal and so for the most effective beam shape and divergence.

a)

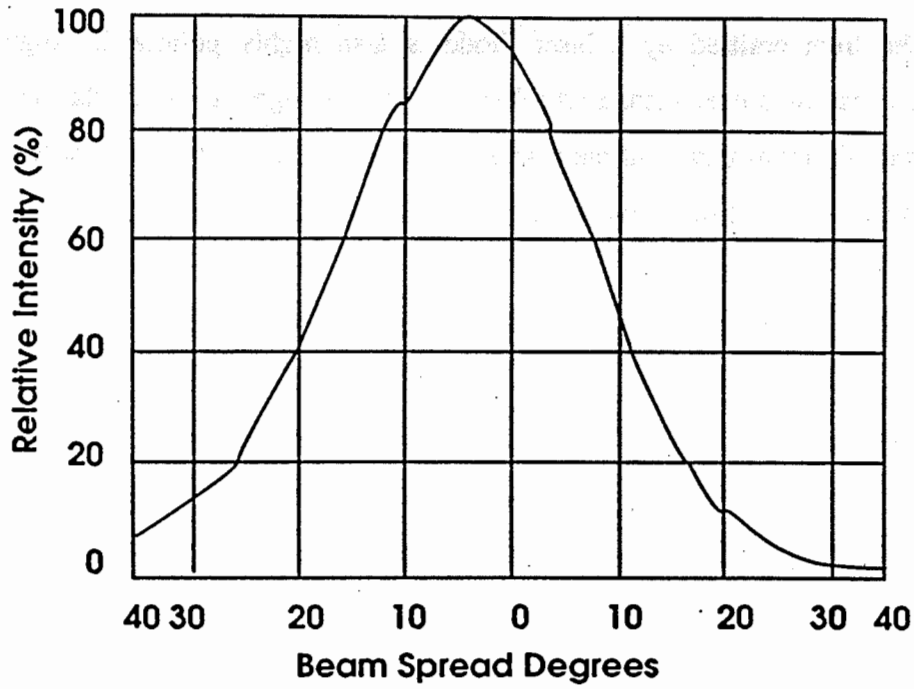

b)

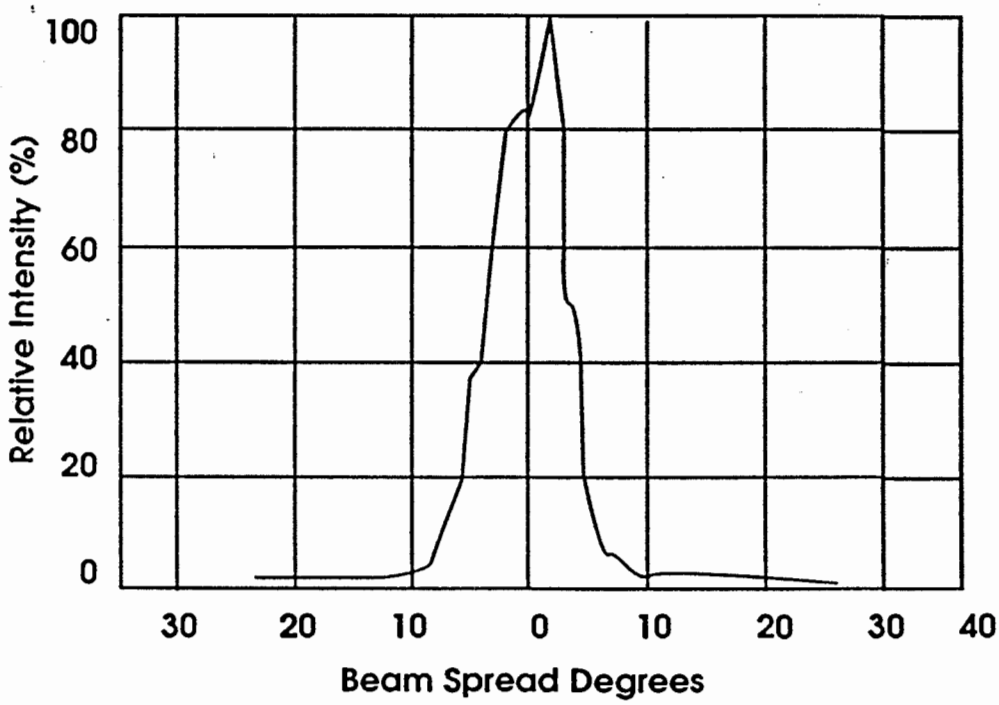

Figure 3.4 Relative intensity versus beam spread for the CVD-97 laser diode a) plane normal to junction and b) plane parallel to junction.

The light emitted by a laser diode is also highly polarized. Figure 3.5 shows the normalized output power measured when the emitted light is passed through a polarizer. The ratio of the minimum power to the maximum is 2.5 % giving a 97.5 % polarization. As will be discussed in section 9, this characteristic might be helpful for the design of the final system.

3.2 THE OPTICAL RECEIVER.

The main component of the optical receiver is the avalanche photodiode detector. The detector is the model C30950E from EG&G, and the operating bias voltage is 373 V at 22° C. The detector's maximum sensitivity occurs at around the same wavelength as the laser diode emission, e.g. 860 nm (see figure 3.6).

To decrease the noise induced by the sunlight or by the cars' headlight emission light, we passed the received light through a laser line filter. This filter has a maximum of transmission at 860 nm and the window is 10 nm wide (3 dB of attenuation). The maximum of transmission of this laser line filter is 50 % but laser line filters of transmission greater than 80 % could be fabricated at a low cost in mass production (we can produce such filters here at NOI).

Since the laser diode wavelength increases with temperature, we adjusted the laser diode temperature to match the laser line filter's peak transmission. Figure 3.7 shows the return signal from a fixed target (in mV) when the laser diode temperature is varied. The optimum temperature is found to be around 22°C. This will then be the selected temperature on the thermoelectric cooler.

Another very important component of the optical receiver is the focussing lens (see figure 3.1). Two parameters are important in choosing that lens. First, the greater the diameter of the focussing lens will be, the higher the received signal will be. There is of course a practical limit to the lens diameter since we want to build a hand hold system. We then have limited the focussing lens diameter to 10 cm (78,5 cm^2 area).

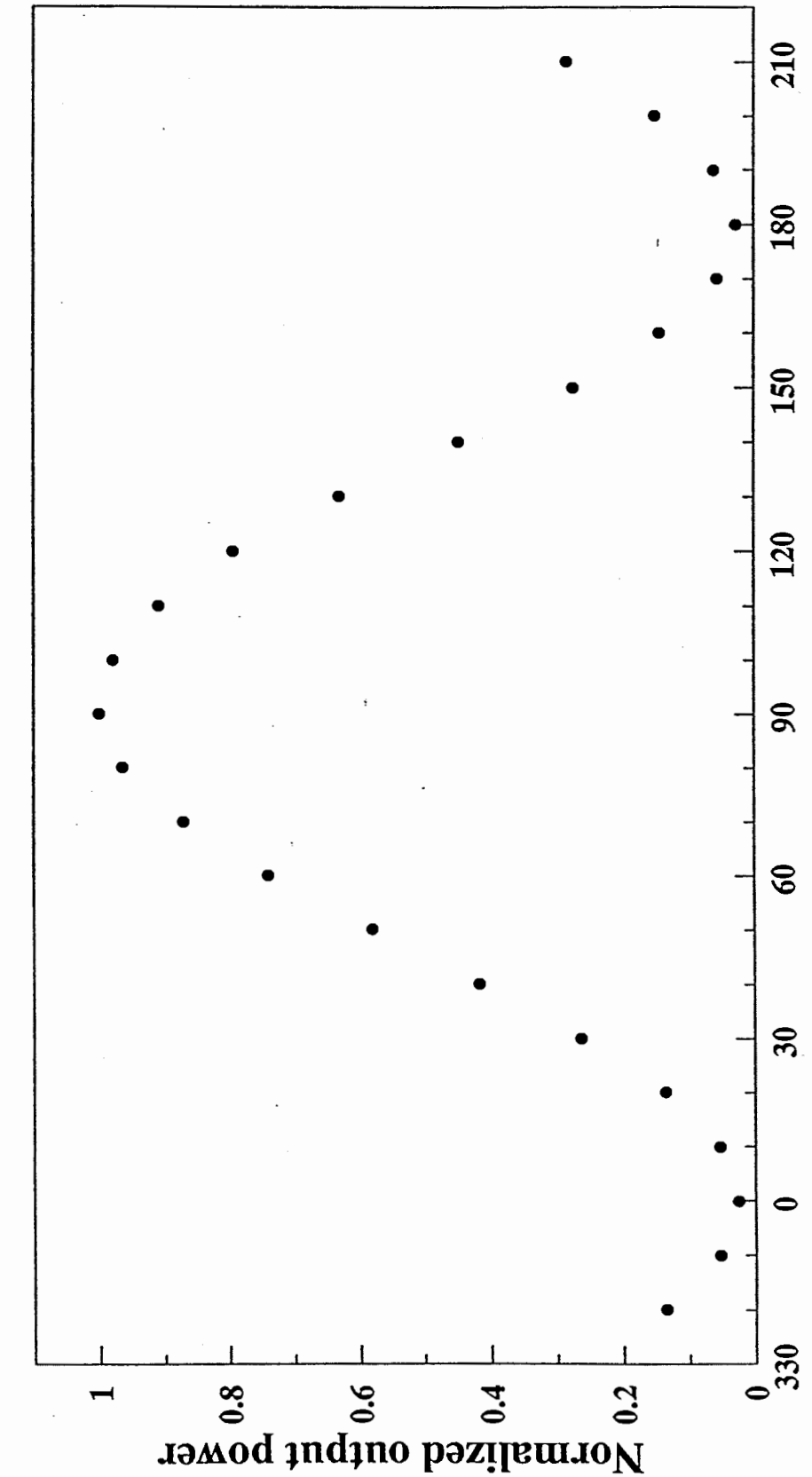

Figure 3.5 Normalized output versus polarizer angle.

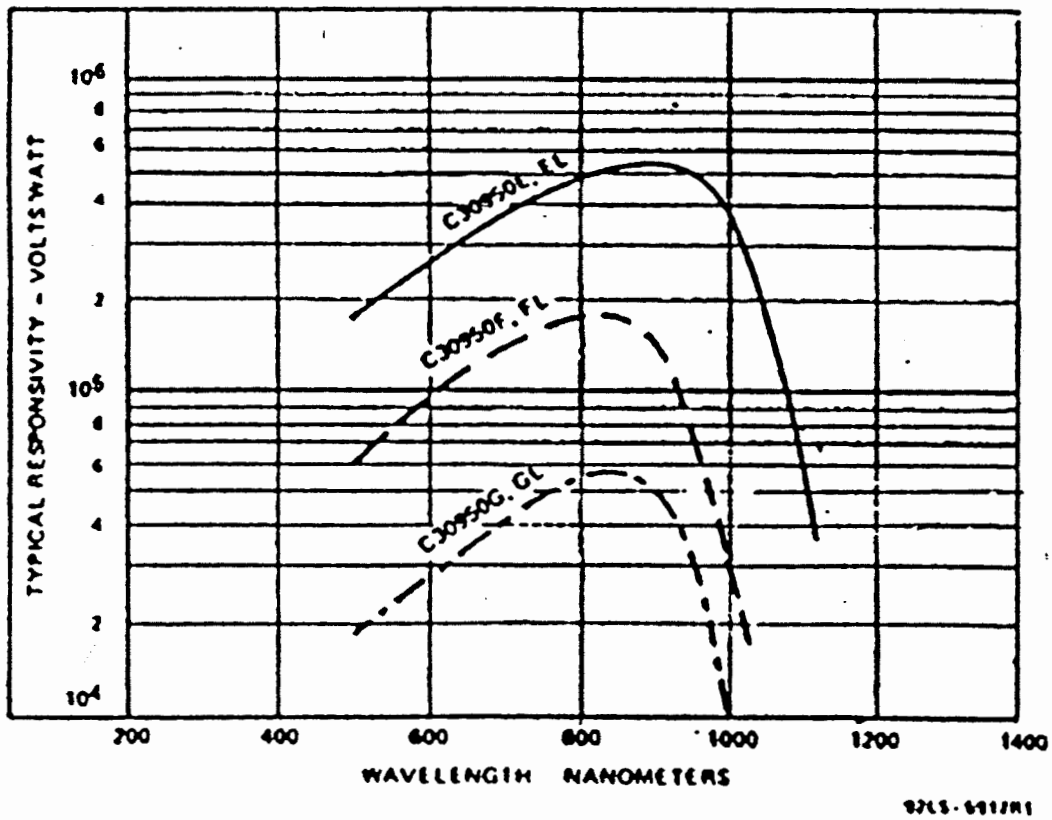

Figure 3.6 Typical spectral responsivity characteristics (our detector is a C30950E).

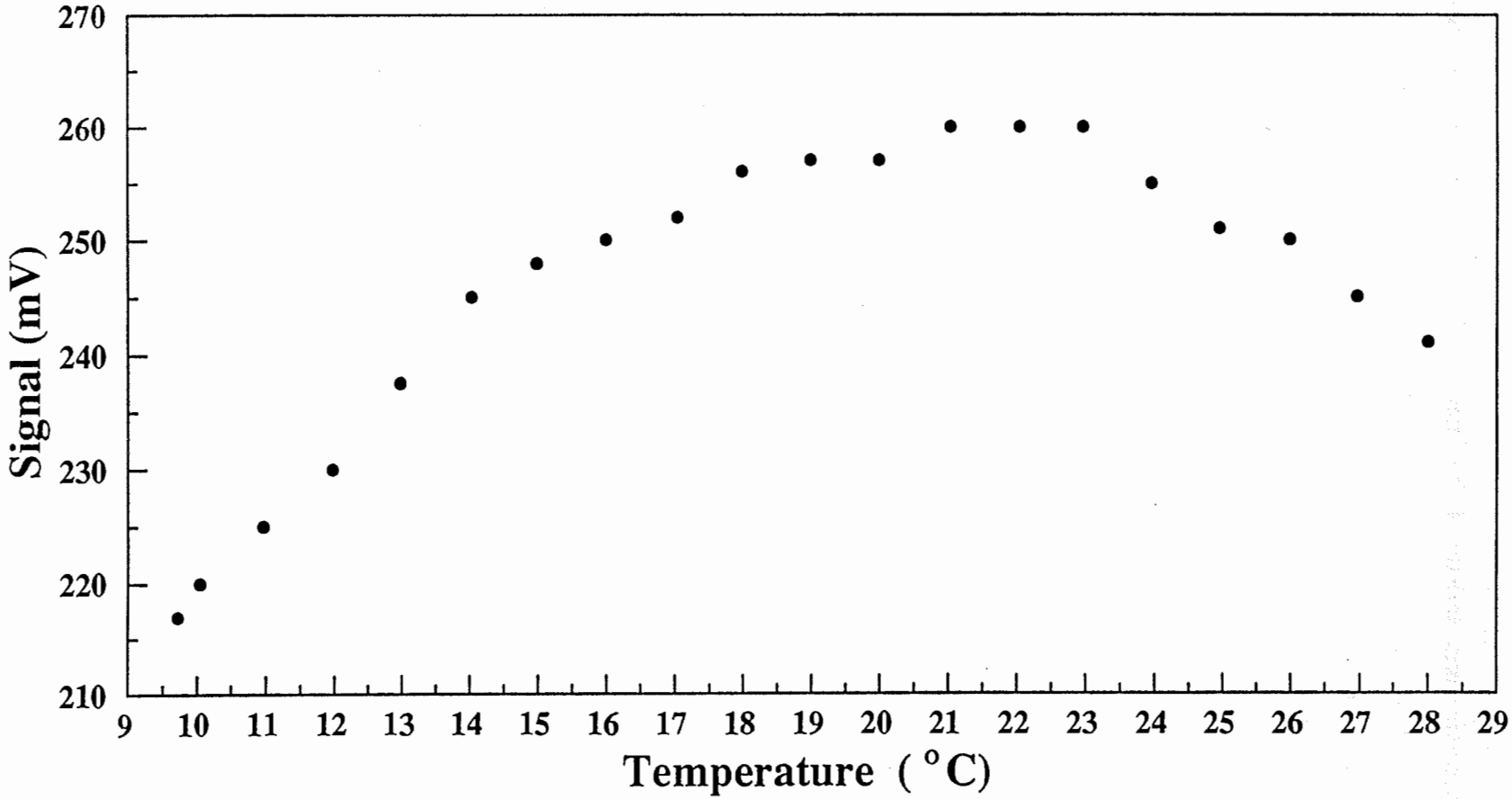

Figure 3.7 Received signal (in mV) from a fixed target versus temperature of the laser diode.

The second important characteristic of the focussing lens is its focal length, especially when the detector surface is small. In our case, the avalanche photodetector surface is 0.8 mm in diameter. It is then seen that if the image on the detector is larger than 0.8 mm, we will loose power. The image size can be calculated using equation 3.2 when the focal length and the diverging angle are known. Ideally, the diverging angle of the received beam can be approximated to be the same as the emitted beam. But, since the emitter and detector are not colinear in our set-up, there is a parallax angle added to the diverging angle. To minimize that angle, we laterally displaced the detector with respect to the receiving lens' center in such a way that no parallax was seen at a distance of 250 m. Then for shorter or longer ranges, the parallax angle is increased. Note that for ranges longer than 250 m, the parallax angle is always small compared to the diverging angle. After we chose the collimating system in section 4, we will be able to calculate the maximum focal length to be used in order to focus all the received energy on the detector surface.

4. FIELD TESTS RESULTS.

We will now present the field test results obtained during the course of the development of the laser based traffic radar. Section 4.1 will first discuss the atmospheric propagation. Then, we will present different collimating geometries in section 4.2 and the receiving optics will be chosen in section 4.3. Section 4.4 will present and discuss the best field test results obtained up to now.

4.1 ATMOSPHERIC PROPAGATION.

Light of different wavelengths is transmitted (or absorbed) differently when it propagates through the air. Moreover, humidity and dust content, as well as temperature and other characteristics of the air do affect the propagation at a fixed wavelength. Unfortunately, we cannot control those parameters, however, we can choose a laser diode with a wavelength corresponding to the highest atmospheric transmission possible to partially overcome this problem.

Laser diodes of lower cost (for a fixed power) are currently available in the 800 to 920 nm range. Figure 4.1 shows the atmospheric transmittance for a 1 km distance in the 800 nm to 950 nm range. The top curve shows normalized results while the bottom one shows the real transmittance. Of course fog, rain or dust in the air will decrease the transmittance.

On figure 4.1, an "atmospheric window" is seen in the 860 to 890 nm wavelength range. Since the 890 wavelength is more eye-safe (for the same power) than the 860 nm, the ideal laser diode wavelength would be 890 nm. In fact, the eye-safety regulation allows a 15 % greater power for the 890 nm wavelength than for the 860 nm. Nevertheless, a 860 nm laser diode was used in the laboratory prototype due to off-the-shelf availability reasons. The increase of "eyesafe" power associated with the use of 890 nm laser diode should be considered during the design of the industrial prototype.

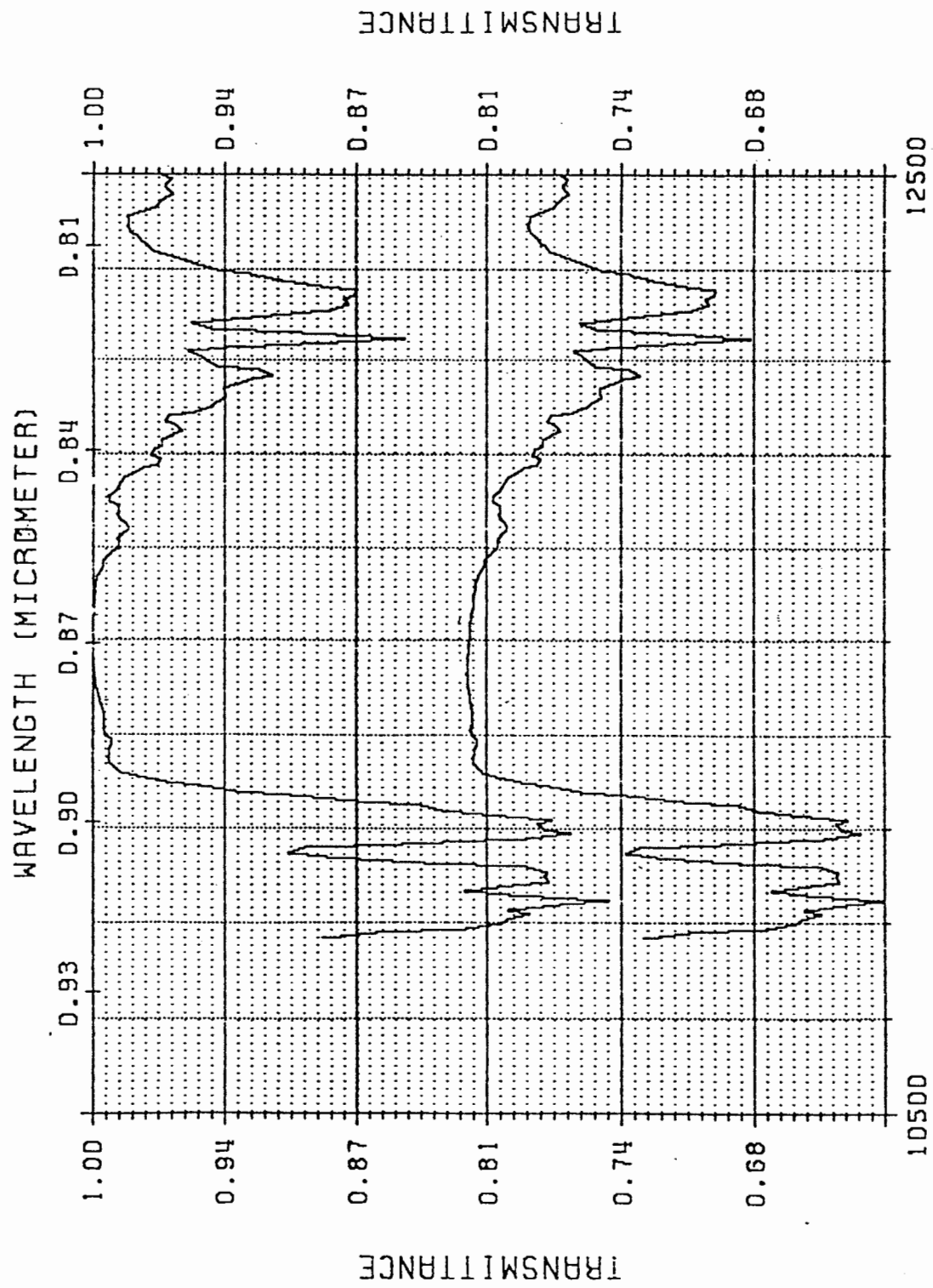

Figure 4.1 Transmittance in a clean atmosphere versus wavelenght for a 1km distance.

4.2 COLLIMATING SYSTEM.

In order to get the highest return signal, we performed field tests with three different collimating systems. From equation 3.2, we know that the longest the focal length is, the smallest the beam divergence will be for a same light source diameter. But in our case, the light source is rectangular and its size is 380 x 2 μm.

The first two systems used were intended to collimate light on one axis and to let it diverge in the perpendicular axis. Moreover, the diverging axis was chosen to be the horizontal one since a car is wider than high because of the windshield which is not reflecting at right angle. Those two systems simply used single spherical lenses. The first system used a 5.1 cm diameter lens with a 5.1 cm focal length. The other was a 10.2 cm diameter Fresnel lens with a 12.7 cm focal length. The third collimating system was composed of a collimator of 1.2 cm equivalent focal length and of a set of two cylindrical lenses of 60 cm equivalent focal length.

With those three collimating systems, we first shot on a Honda Accord 1989 car (blue) with the traffic radar set-up of figure 3.1. This car has retractable headlights. At a distance of 300 m, the return signal measured was at least 3 times lower when the headlights were retracted than when they were out. The car did not have a front license. This confirms that the headlights are the place to aim at when measuring an incoming car, especially a car profiled like the Honda Accord.

We also measured the received signal level (with the same set-up as figure 3.1) from the same car with headlights out at different ranges from about 60 m to a 300 m range. Figure 4.2 shows the results for the 3 collimating systems where the Fresnel lens, the 5.1 cm diameter lens and the collimator + cylindrical lenses are respectively called system #1, #2 and #3. On this figure, not only the signal level is important but also the slope of the curve. In fact the signal level, S, is proportional to the range, R, at the slope power:

$$S \propto P_0 k R^m, \tag{4.1}$$

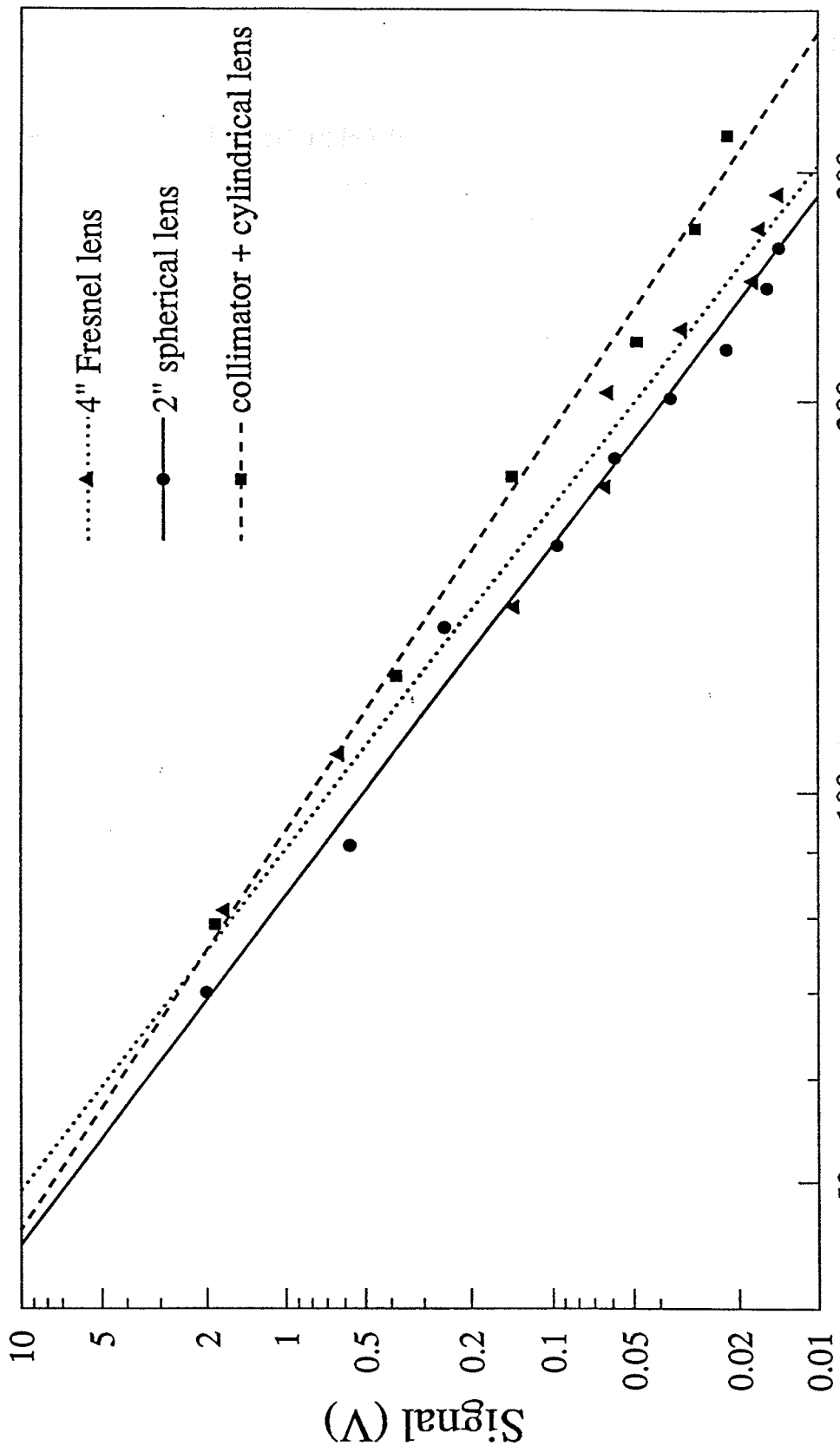

Figure 4.2 Photodetector signal versus range (m) for three different collimating systems.

where P_0 represents the initial output power, k is a factor taking into account the beam spot size or shape on the target and also the target's reflectance, and m is the slope of the curve on figure 4.2. The smallest the slope is, the slower the received signal will decrease with the range since the slope is always negative.

On figure 4.2, we clearly see that the best results were obtained with system #3 (collimator + cylindrical lenses). The received signal is always greater for a given range and the slope of the curve is m = -3.25 compared to m = -3.71 for system #2 and m = -3.80 for system #1.

We must also say that the divergence obtained with system #3 is the smallest and since headlights are the most contributing components to the return signal, the smallest spot size at a given distance is most likely to give the greatest return signal given the small area of a headlight. That is exactly what was observed. The beam diameter at 60 m was around 20 cm and the beam was almost circular. By extrapolation we deduce that the beam diameter was around 1 m at 300 m and around a car's width at 500-600 m. Therefore, the next measurements will be taken with collimating system #3.

4.3 THE RECEIVING SYSTEM.

To recoil the highest signal as possible, we needed to use the greatest lens diameter possible. As already mentioned, we limited the lens diameter to 10.2 cm for apparatus size considerations. Moreover, from equation 3.2 it was seen that the shortest the focal length is, the smallest is the image size.

To do our experiments, we had two 10.2 cm diameter lenses. Lens #1 was a biconvex glass lens of 15 cm focal length. Lens #2 was a Fresnel lens of 12.7 cm focal length. From section 4.2, we can approximate the divergence of the beam to be

$$\theta \approx (0.2/60) \approx 3.3 \text{ mrad} \approx 0.2^\circ \quad . \tag{4.2}$$

From equation 3.2, the image size, D, with lens #1 should be

$$D = \theta f = 3.3 \text{ mrad x } 15 \text{ cm} = 0.5 \text{ mm} \quad , \tag{4.3}$$

and for lens #2, the image size should be

$$D \sim 0.42 \text{ mm} \quad .$$

Since both lenses give an image spot size smaller than the detector surface diameter of 0.8 mm, both lenses should give the same results. It was not the case. Lens #2 gave twice as much signal as lens #1. This is mostly explained by the shape of lens #1 which is biconvex. Biconvex lenses are not well suited to focus an almost collimated beam onto a point. They induced spherical aberration which distort the beam, induce losses of power and produce images greater than predicted by theory. Moreover, the Fresnel lenses are well suited for focussing monochromatic light onto a point and the unit price is around three times lower than the glass lens (lens #1). So, from now on, we will use a 10.2 cm diameter Fresnel lens as the focussing lens (see Figure 3.1).

4.4 FIELD TEST RESULTS AND DISCUSSION.

The optical field tests were performed with the set-up of figure 3.1. To track a moving car at any time, we mounted the optical set-up on a tripod. Figures 4.3 and 4.4 show two different pictures of the optical system. Moreover to bring the system wherever we wanted, we placed it on the back of van. Figure 4.5 show a picture of the laser radar when operated and placed into the van. The set-up length and width are respectively 90 cm and 20 cm. Of course the prototype size can be reduced with proper optical design. During the optical field tests, the received signal was directly transferred to an oscilloscope and then the speed of the aimed car was not available. But the shape, signal level and approximate range were measured. The range, R, was deduced from the time of flight of the laser pulse:

$$R = c\,t / 2 \ , \qquad (4.4)$$

where c is the speed of light. The time of flight was directly measured with an oscilloscope. We must add that the return signal shape has been observed to be unchanged after return, no matter the target measured. This is an important result since we can be sure that a signal processing unit can be optimized to treat a very well definite signal waveform.

Also, to ease the tracking of moving cars, we add a rifflescope aligned with the laser beam to the set-up. The tracking of moving cars was then easy to do. When the car was moving forward, we aimed at a headlight and when it was receding, we aimed at a parking light.

Measurements were taken during different days and weather conditions and at different time of the day. We observed that the weather, e.g. humidity of the air and wind (or dust content) affects the performances of the laser radar. The best ranges obtained, e.g. the maximum ranges at which we still distinguished the received signal on the oscilloscope screen, was around 700 m for an incoming car and more than 1.2 km for a receding one. (The car then used was a Volkswagen Golf.) In that particular case, the measurements were taken at sunset without any wind and the air was dry.

We also performed measurements at noon under strong wind condition and high degree of humidity in the air, a decrease of the maximum ranges of about 20% was then observed. Unfortunately, we did not check when it was raining. The range decrease was due to both an higher background noise from the sun which could probably be eliminated and to a lower transmittance in the air at the working wavelength which cannot be eliminated.

As already stated in the preliminary report, a minimal signal-to-noise ratio must be obtained before we can ensure a good precision on the measures. The next 4 sections will be devoted to the presentation of the signal processing unit and section 9 will present two possible designs for an industrial laser radar prototype.

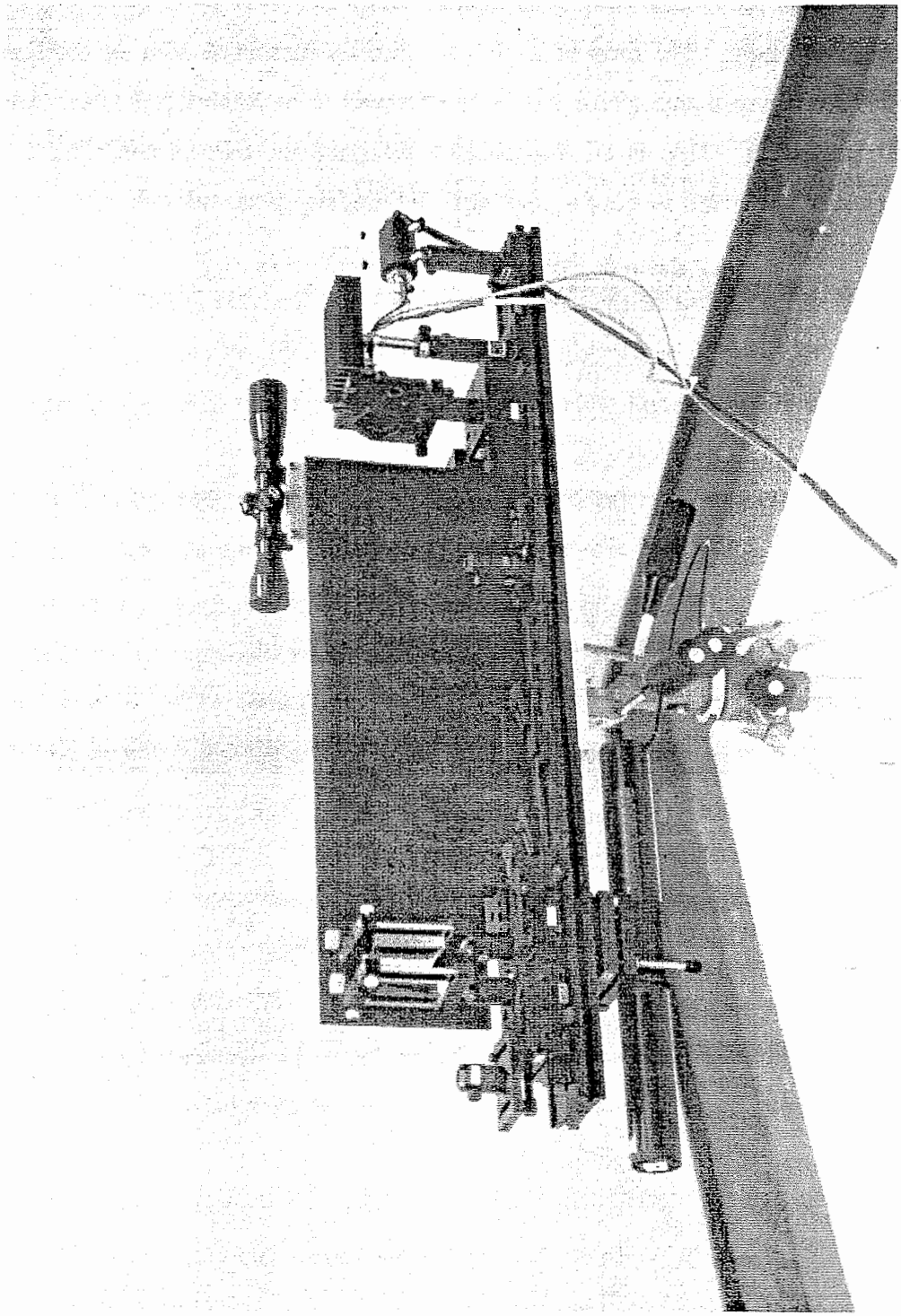

Figure 4.3 Laser radar optical set-up mounted on a tripod (emitter side).

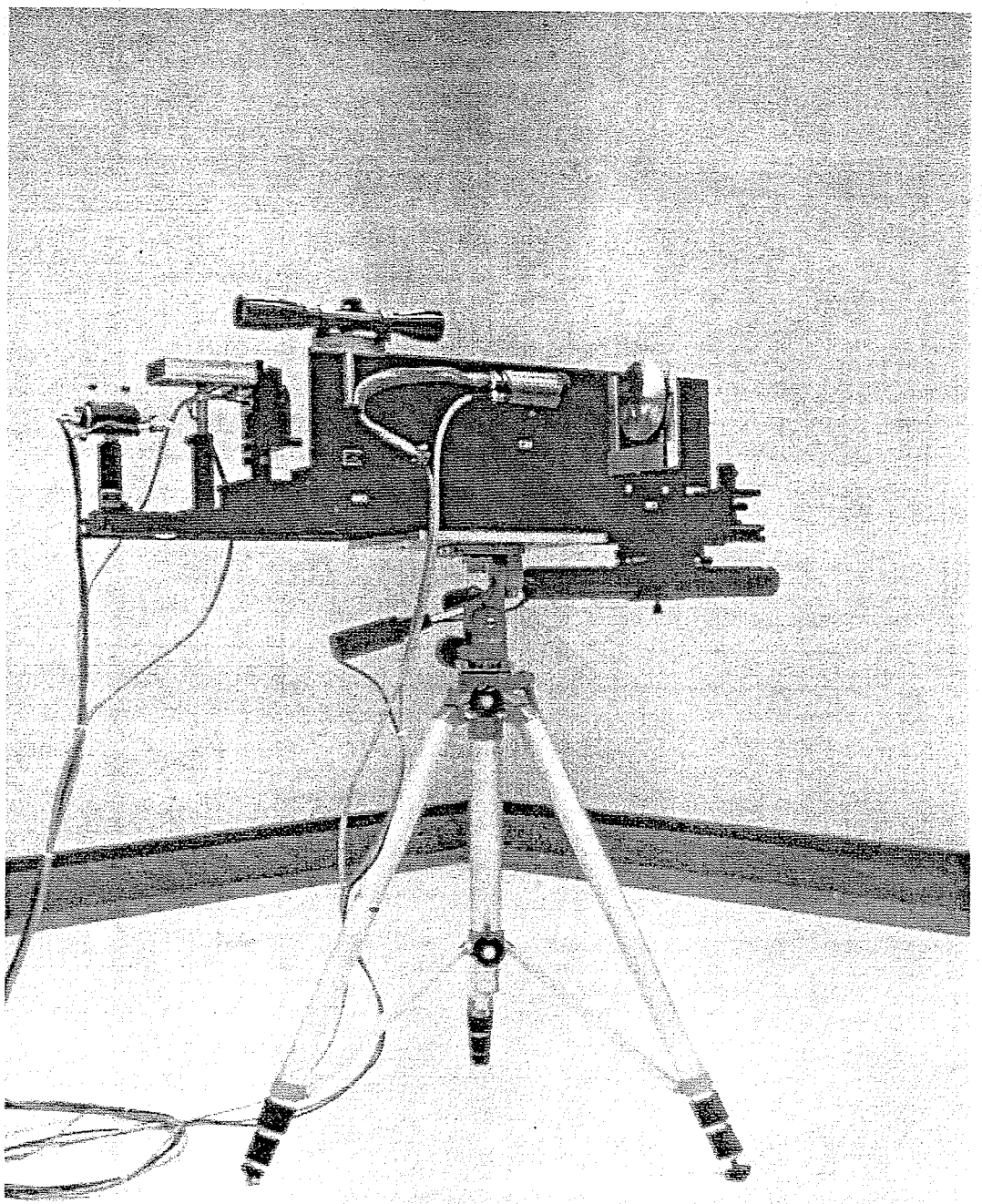

Figure 4.4 Laser radar optical set-up mounted on a tripod (receiver side).

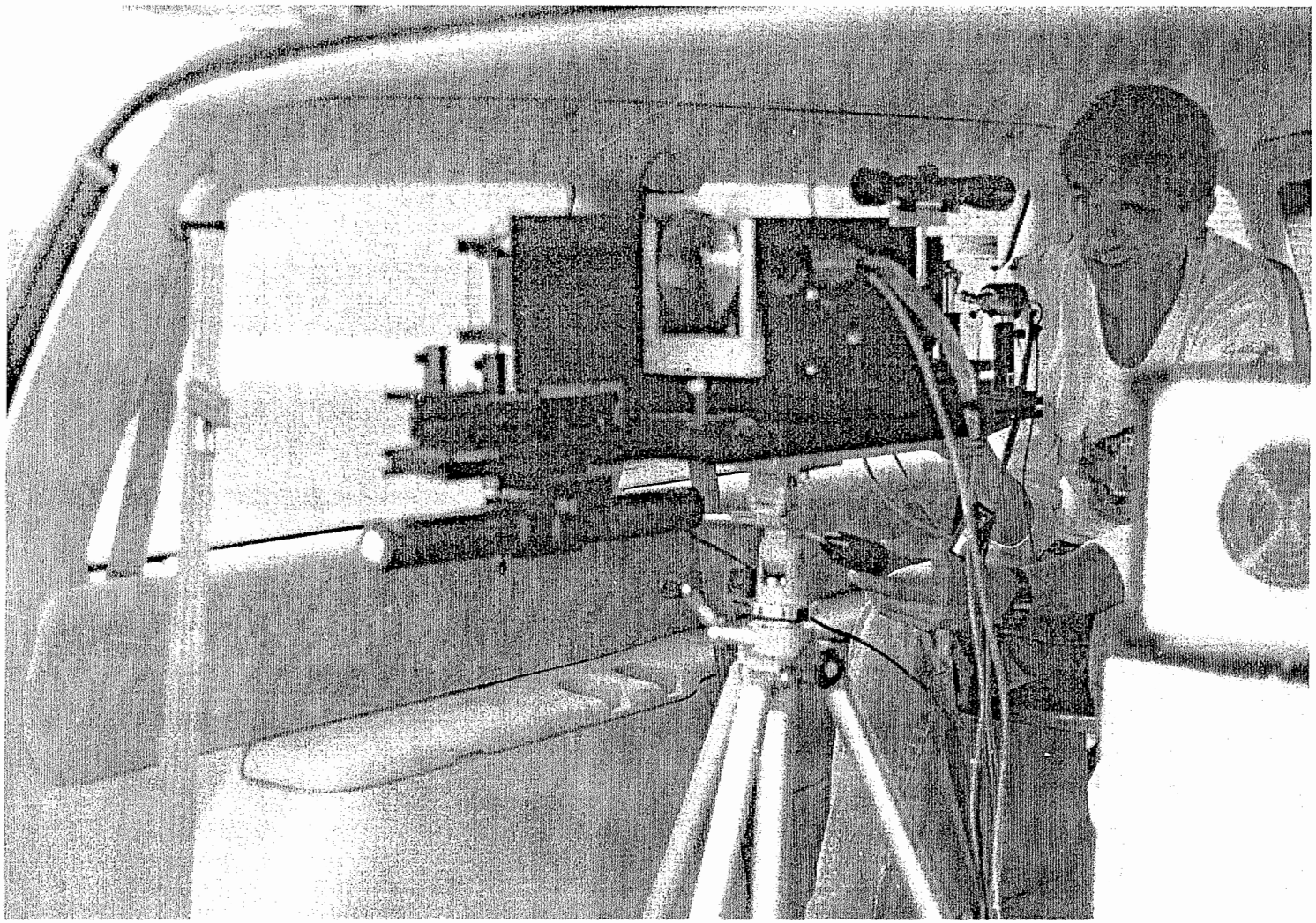

Figure 4.5 Laser police radar operated from the back of a van.

5. SIGNAL PROCESSING OVERVIEW.

This second part of the present report is devoted to the electronics and signal processing aspects of the laser traffic radar prototype. Four topics will be discussed, each of these subjects being covered by a specific section. The four topics are a brief review of the theory, the actual implementation in hardware and software, the results achieved and a list of suggested improvements.

5.1 THEORY REVIEW.

The feasibility study [1] submitted in April suggested that the radar should be built using a time of flight (TOF) approach. We recall that the basic idea behind this approach is the fact that, the speed of light being a constant known very precisely, the time it takes for a small packet of light (a pulse) to cover the distance to and fro between two objects can be used to assert their relative range. Since the relative velocity of these objects is simply the rate of variation of their relative range over time, one quickly understands that two range measurements at different instants can yield the speed. Put into equation, this principle can be expressed by:

$$v = (R_1 - R_2) / T = c\ (\delta_1 - \delta_2) / 2T \qquad (5.1)$$

where v is the relative speed; R_1 and R_2, the ranges at two different instants t_1 and t_2; T, the time interval expressed in seconds between t_1 and t_2; c, the speed of light and δ_1 and δ_2 the back and forth time of flight for the pulses launched at t_1 and t_2 respectively. In order to provide a better feeling of the principle involved, the mechanism is depicted in figure 5.1. From this figure and from equation 5.1, one sees that the velocity measurement task has been progressively reduced to a range measurement and then to a time interval measurement.

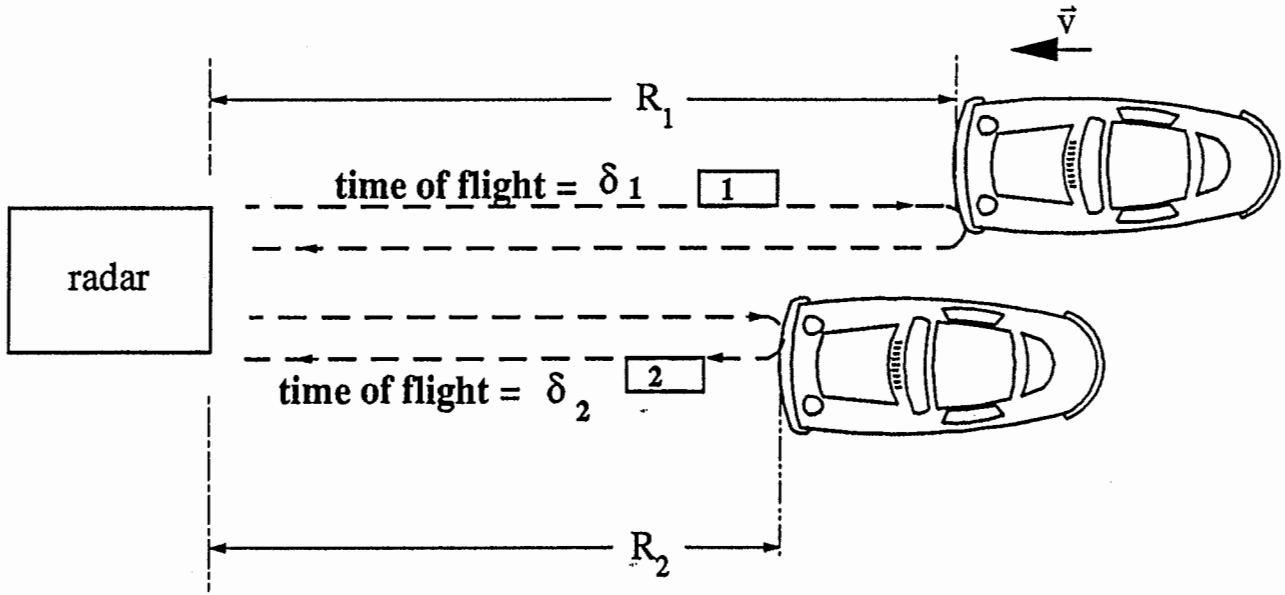

$$\bar{v} = \frac{c}{2\overline{T}}(\delta_1 - \delta_2)$$

with

$\overline{T}$ acquisition time
δ round-trip time of flight

Figure 5.1 The time of flight technique.

Until now, we have assumed that the noise would not influence the precision to which the echoed pulse time-of-arrival could be measured. However, even with an infinite resolution time-interval meter, the measurement would nevertheless be susceptible to errors. This is partly due to the noise present in the signal and partly to the finite bandwidth of the pulse (e.g. its rise-time). Thus, the achievable accuracy is not only function of the time measurement accuracy but also of other parameters of design. Consequently, we may wonder what kind of output precision can be expected from a set of parameters leading to a certain time resolution.

We have already presented an equation enabling us to answer this question. This equation, presented in the first report related the achievable time measurement accuracy to all the fundamental parameters of our experiment (i.e. the pulse width, its rise-time and the signal-to-noise ratio (SNR)). The formula then presented also accounted for an enhancement of resolution achieved through averaging over N pulses. We recall that a simple averaging over N independent measurements can lead to a $\sqrt{N}$ increase in resolution. In this particular case, the averaging can be accomplished by sending the pulses in two bursts of N pulses at both ends of the acquisition interval T. This technique is best explained graphically as is shown in figure 5.2.

While suitable for a theoretical analysis, the equation can be rewritten into a form more compatible with experimental measurements. Thus, we can write:

$$\sigma_\delta \geq \left(\frac{N_o t_r}{NA^2}\right)^{1/2}, \tag{5.2}$$

where σ_δ is the time jitter (the accuracy), N_o the noise spectral density, A the voltage amplitude of the received pulse, N the number of readings averaged and t_r the pulse risetime. We also note that the equation has been rewritten with an inequality sign to underline the theoretical lower bound nature of the equation. By inspection of equation 5.1, we also notice that the speed accuracy is proportionnal to twice the time accuracy. Thus, the speed uncertainty may be described in the following way:

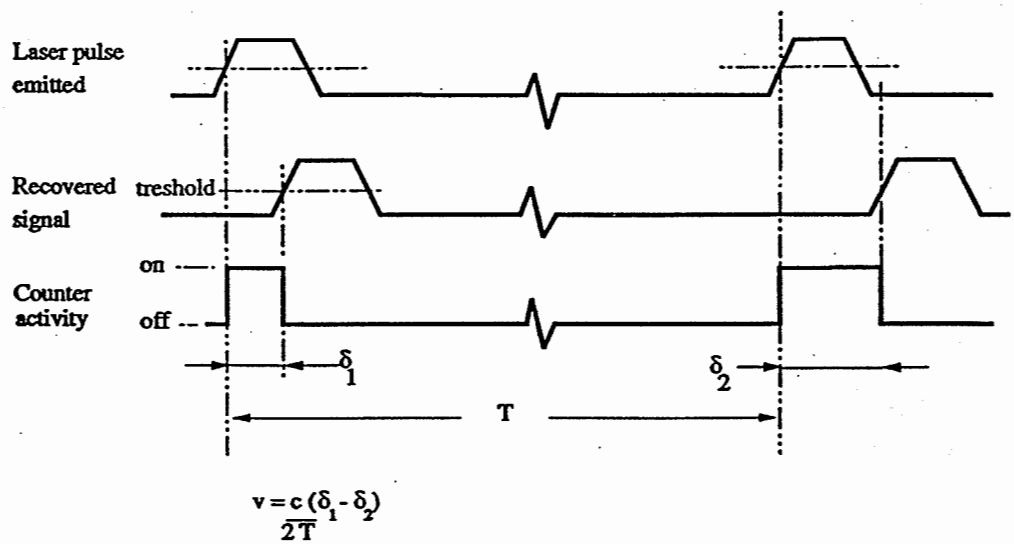

Figure 5.2.a The time of flight timing diagram.

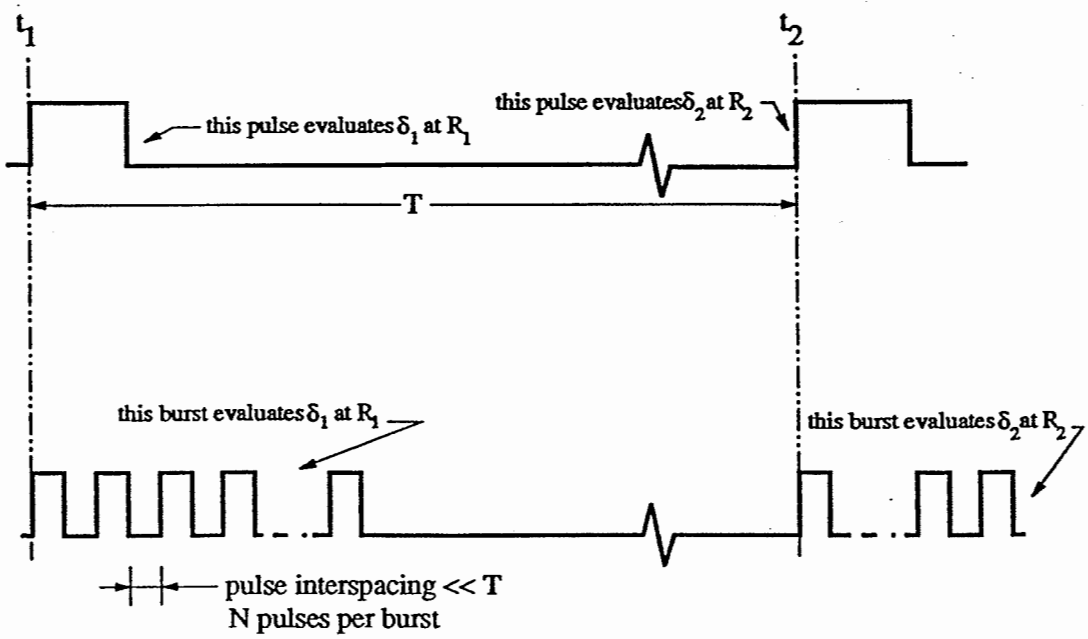

Figure 5.2.b Extension of pulse time of flight to a burst.

$$\sigma_v = \frac{2\sigma_\delta \cdot c}{2T} = \frac{\sigma_\delta \cdot c}{T} \quad . \qquad (5.3)$$

Equation 5.3 clearly indicates that the speed resolution is linked to the time interval between the two bursts of pulses (assuming averaging will be used). In the feasibility study, we had assumed a 1s overall acquisition time. Thus, sticking with this value, all of our experiments were accomplished with a 1s acquisition time. The response time of the radar, including computing overhead was therefore slightly larger than 1s. However this value was arbitrarily set to ease the development of this first prototype. An actual device should have a smaller response time as will be discussed later on.

5.2 AN EXAMPLE.

Before proceeding on to the explanation of the actual implementation of the time of flight, let us look at an example to get an idea of the magnitude of the numbers involved.

We first assume our target is 300 meters away and incoming at 60 kmh^{-1}. As discussed above, the time interval between the emission of the two bursts at time t_1 and t_2 is 1s. When the first burst is sent toward the target, the car is 300 m away. Since the pulses in the burst are close in time, we can make the hypothesis that the car do not move significantly over the burst duration, that is all the pulses in one burst have the same time of flight. Thus the back and forth time of flight for every pulse in the burst is:

$$\frac{2R_1}{c} = 2.000\mu s.$$

At time t_2 (e.g., one second later) when the second burst is emitted the car has moved by 1s · 60 kmh^{-1} = 16.67 meters. Thus, the new range R_2 is 283.3 meters. The new time of flight is now 1.887 μs and the difference $\delta_1 - \delta_2$ becomes 111.3 ns.

Now, if we want to achieve a precision of ± 0.5 kmh^{-1}, the difference in the time of flight must be evaluated to better than one part in 60/0.5 or 1:120. The required resolution is then found to be 1/120 · 111.3ns or 928 ps. Finally since the errors of both evaluations of δ (δ_1 and δ_2) may have a cumulative effect, the value must be divided by 2 and the required temporal resolution becomes 464 ps. Finally, averaging over a hundred pulses reduce the constraint by an order of magnitude and we finally get a required resolution of 4.64 ns.

6. IMPLEMENTATION OF THE CONCEPT.

This section will briefly describe the actual software and hardware implementations of the laser traffic radar. We will also take a closer look at the most important subsystems and explain their interactions. Basically, the processing electronics can be divided into four main blocks. First, there is the system core, composed of a time-interval meter used to evaluate the time of flights. This meter is started whenever a laser pulse is sent and stopped upon detection of the returned energy. Then, there is the photodetector and its associated electronics that detect the incoming energy and provide the stop signal to the time-interval meter. Finally, the remaining blocks are the laser diode with its trigerring circuitry and the computer, responsible for the calculations, the synchronization and the user interface. The general block diagram of the radar showing the main components and their interaction is provided in figure 6.1.

6.1 TIME-INTERVAL METER.

Of course, one can think of many ways to achieve a time measurement by electronic means. However, there are fundamentally two ways to go: either in an analog or digital fashion. The analog solution can yield impressive results but the design effort is a lot more considerable and the results less easily predictable than with an all digital approach: a digital design either work or do not whereas an analog system has more "degrees of functionality". Since both techniques lead to adequate results in this case, it was decided to design around a digital approach for the sake of simplicity.

Our time-interval meter is built around a counter which increments the value stored in a register at every tick of a clock. Of course, the value in the register is set to zero before every measurement. The counter is started upon reception of a "start" signal synchronized with the emission of a laser pulse. Upon arrival of the echoed signal, the received pulse is filtered, amplified and level discriminated to provide a suitable "stop" signal to the counter.

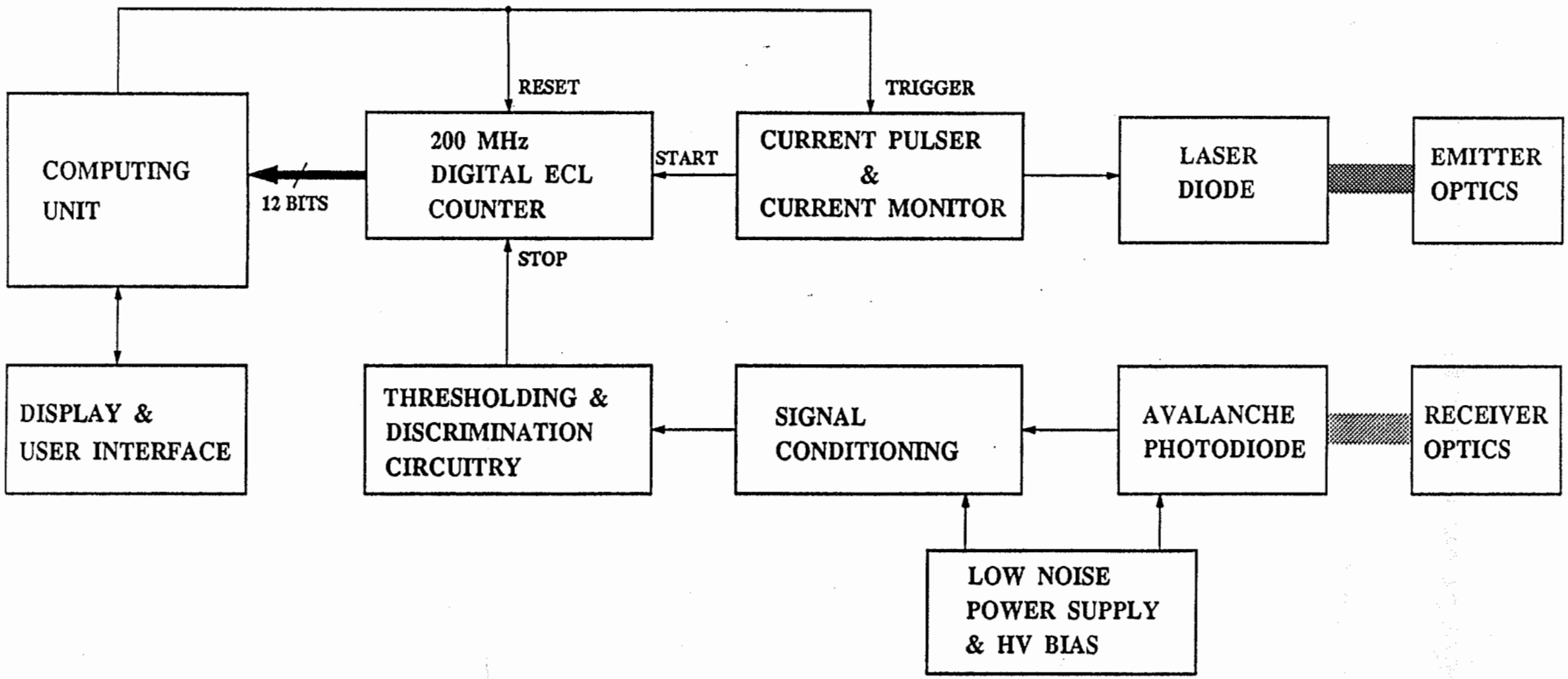

Figure 6.1 Laser traffic radar block diagram.

The minimum resolvable time with such a counter is evidently set by the clock period. Since we have seen in the previous section that a 4.6 ns resolution was required (still assuming that 100 pulses were to be averaged), our counter was designed with a clock period as close as possible to the required resolution. The adopted frequency was therefore 192 MHz (5.21 ns resolution) and the design was implemented using a 48 MHz crystal quadrupled to 192 MHz by a phase-locked loop.

Since the original targeted range was about 1 km (back and forth time of flight = 6.67 μs) we needed a counter able to count up to at least $6.67 \times 10^{-6}/5.21 \times 10^{-9} = 1280$. Thus at least 2^{11} levels were required. We decided to use three 4-bit counters cascaded together for an overall 12-bit (2^{12}) readout. Thus, the maximum count was 4095, which amounted to 21.36 μs or about 3.2 kms.

Due to internal propagation delays, the minimum count was found to be around 20 for a minimum range of about 15m. However, to prevent false stops from occuring (possibly generated by reflected light or induced by electromagnetic interferences) the stop signal was inhibited for a short period of time immediately after the launching of a pulse. This stop inhibit was programmable in 20 ns increments up to 300 ns. During the experiments, the stop inhibit time was set at its maximum value. The minimum range was therefore 47 m. In addition, whenever a stop signal failed to be received after about 20 μs, the output of the counter was automatically zeroed, this latter feature to prevent irrelevant readings when the radar wasn't pointed toward a target. Finally complete drawings can be found in Appendix A.

6.2 PHOTODETECTOR/AMPLIFIER CHAIN.

The radar detector is an avalanche photodiode (model EG&G 30950E). The selection of this component follows from a theoretical analysis of the requirements as was explained in the feasibility study. Let us just recall that this detector was selected for its good responsivity and relatively high bandwidth. Following the detector, down the chain, we find the signal conditioning subsystem. This unit is composed of a limiting amplifier inserted between two

passive low-pass high order filters. A limiting amplifier was used to reduce the signal dynamic range at the output of the amplifier. This limiting amplifier had a 40 dB gain (into 50 Ω) and its output power saturated at about 0 dBm (250 mV). Taking into account the filters insertion losses, a detector output signal of about 5-6 mV was required to drive the amplifier into saturation. Since the detector output was limited to 500 mV, we had a constant waveform fed to the thresholding circuitry over a 40 dB dynamic input range. As a consequence, the effect of the variations of input optical power over the time of arrival were attenuated.

Two fifth-order low-pass filters were added before and after the amplifier to limit the noise bandwidth. The two prime sources of noise were the target background and the detector intrinsic noise as we noted that the amplifier contribution was smaller than any one of these other contributions. The filters bandwidths were selected after an FFT analysis of the pulse shape to optimize the SNR ratio, since we had observed that the targets almost invariably led to the same echoed pulse shape. Finally, the level discriminator was a simple comparator with one input set at a fixed level.

6.3 LASER DIODE TRIGGERING CIRCUITRY.

The laser diode emission was controlled via a current pulser manufactured by Power Technology Inc. The pulser output peak current and pulse width were both independently programmable. At the required operating current, the minimum pulse width achievable was about 200 ns with the pulser model we had in hand when the tests were held. The pulse rise time was about 100 ns and a simple TTL signal was required to induce the current discharge through the laser diode. This TTL signal was synchronized with the start signal of the counter.

6.4 COMPUTER SUBSYSTEM.

The data acquisition, the synchronization between the different components and the user interface tasks were all managed by a PC-compatible computer and a digital I/O accessory board. The overall activity was under the control of a small program written in "C", the listing of which

appears in Appendix B. The program was designed to be running idle and was brought into activity by any keyboard keystroke. The velocity and range measurements were then initiated and the results were displayed on the monitor upon completion of calculations. The range displayed was the average of the two range measurements R_1 and R_2.

7. FIELD TRIALS.

This section summarizes the results obtained with the prototype during the field trials. The actual operating parameters are first detailed. Afterwards, the results are presented and analyzed. Finally the results are compared with those theoretically achievable under the operating parameters described.

The field trials were held on a flat road about a kilometer long. Measurements were taken over two days under various sky conditions ranging from sunny to overcast. The measurements were taken on two different cars with drivers alternating between the cars. Thus, while not exhaustive, the field tests were performed under a significant enough number of conditions to assess the radar performances.

A small signal was still echoed by the targets at distances up to about 700 meters when the targets presented a front view while this maximum range was increased to 1100 to 1200 meters when the targets were viewed from the back. However, at these maximum ranges, the signal-to-noise ratio was too low to be of practical use and the measurements were generally achieved at distances of up to 400 and 600 meters when looking at the front and back surfaces respectively.

A sample distribution of the speed values obtained during the field trials is given in figure 7.1. The measurements were taken in batches during a single run of a car and figure 7.1 shows the cumulative data of some of these runs. Obviously, all the measurements whithin one batch (or run) were taken at different ranges. The cars were always moving at the nominal speed of 50 kmh^{-1} as indicated by the cars odometers.

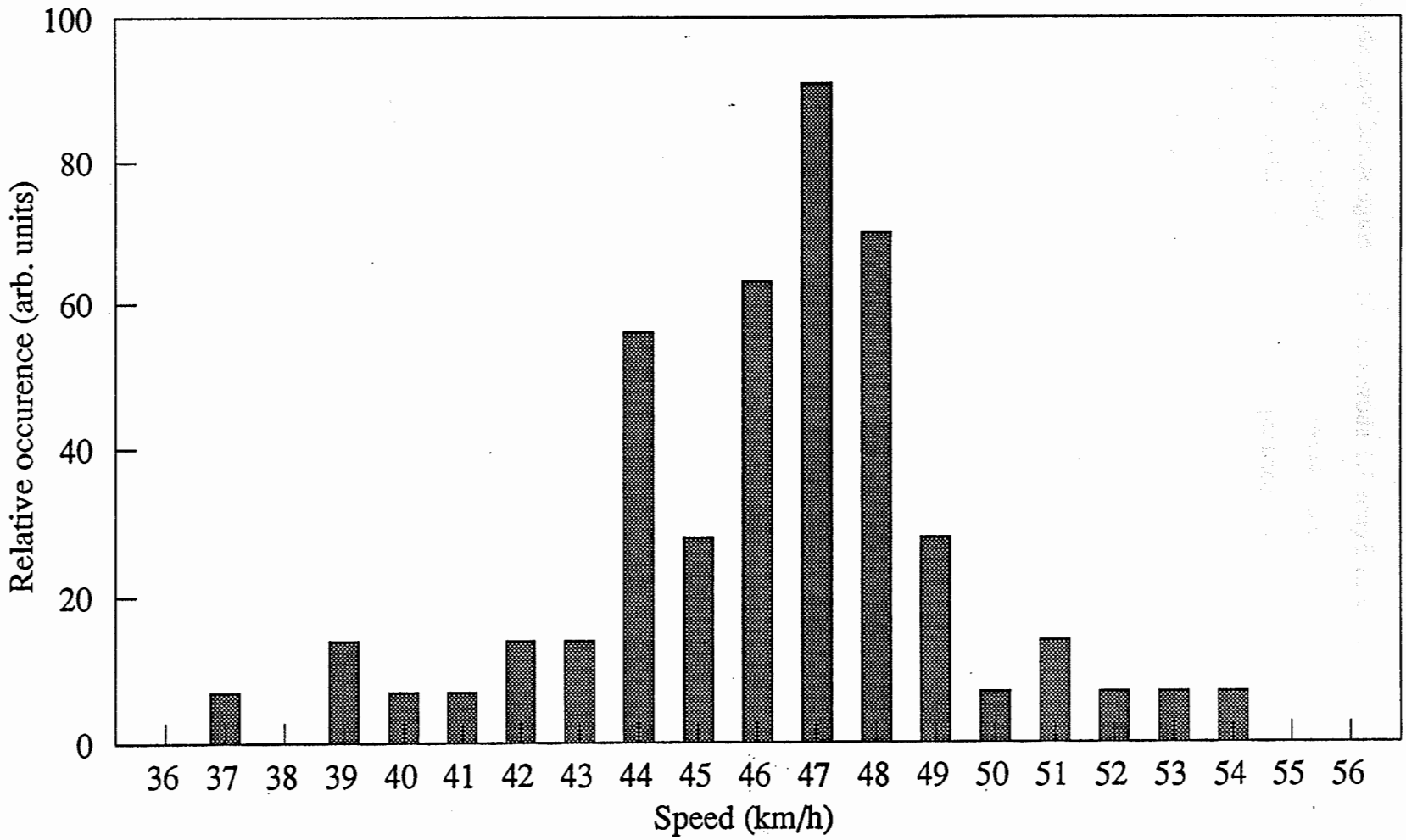

Figure 7.1 Global distribution of speed measurements (the nominal speed was 50 km/h).

Analysis of the data presented in figure 7.1 show that the average speed was about 46 kmh^{-1}; 4 kmh^{-1} away from the nominal value. However, this discreapancy is not considered significant given that no independent way of measuring the speed was available. In addition, a slight error in the evaluation of the exact time interval T may also explain a part of this offset. As might be expected from moderate to high signal-to-noise ratios conditions, the distribution exhibit a roughly gaussian profile with a standard deviation of 3.2 kmh^{-1}.

Figures 7.2 and 7.3 show the same data presented in different ways. First, figure 7.2 shows data for individual runs (e.g. many readings taken during the same car movement sequence). For illustration purposes, the speed values have been regrouped in bins. Thus, the value under the label 47 actually represent the number of occurences of the 46, 47 and 48 kmh^{-1} speed values. The mean velocity for every run fluctuated between 45.3 and 47.5 kmh^{-1} while the standard deviation ranged from 2.1 up to 3.4 kmh^{-1}. These variations in the standard deviation may be explained by the relatively low number of samples in each run (generally between 10 and 16).

Figure 7.3 displays the same values using the range parameter instead of the run number. The readings were partitioned into groups according to the range at which they were taken. Again, no significant tendency emerges from this data. We must therefore conclude that within the scope of our evaluation, the range does not significantly influence the accuracy. As would indeed be expected, we nevertheless believe that a relationship between range and accuracy would show up with a more precise device.

For reasons mostly out of our control, the parameter of the actual prototype were quite different from those originally planned (the laser diode pulser purchase especially for this project was delivered too late to be of any practical use). Yet, using equation 5.2 and putting in the actual parameters we can find the resolution that could have really been expected. The noise spectral density N_o was estimated to be about $1.8 \times 10^{-11} V^2/HZ$ (15mVrms). The bandwidth was roughly 12 MHz (brickwall equivalent). Furthermore, the signal was tresholded at 70 mV and the number of samples was fixed to a 100. Finally, the pulse rise-time was 100 ns. Therefore,

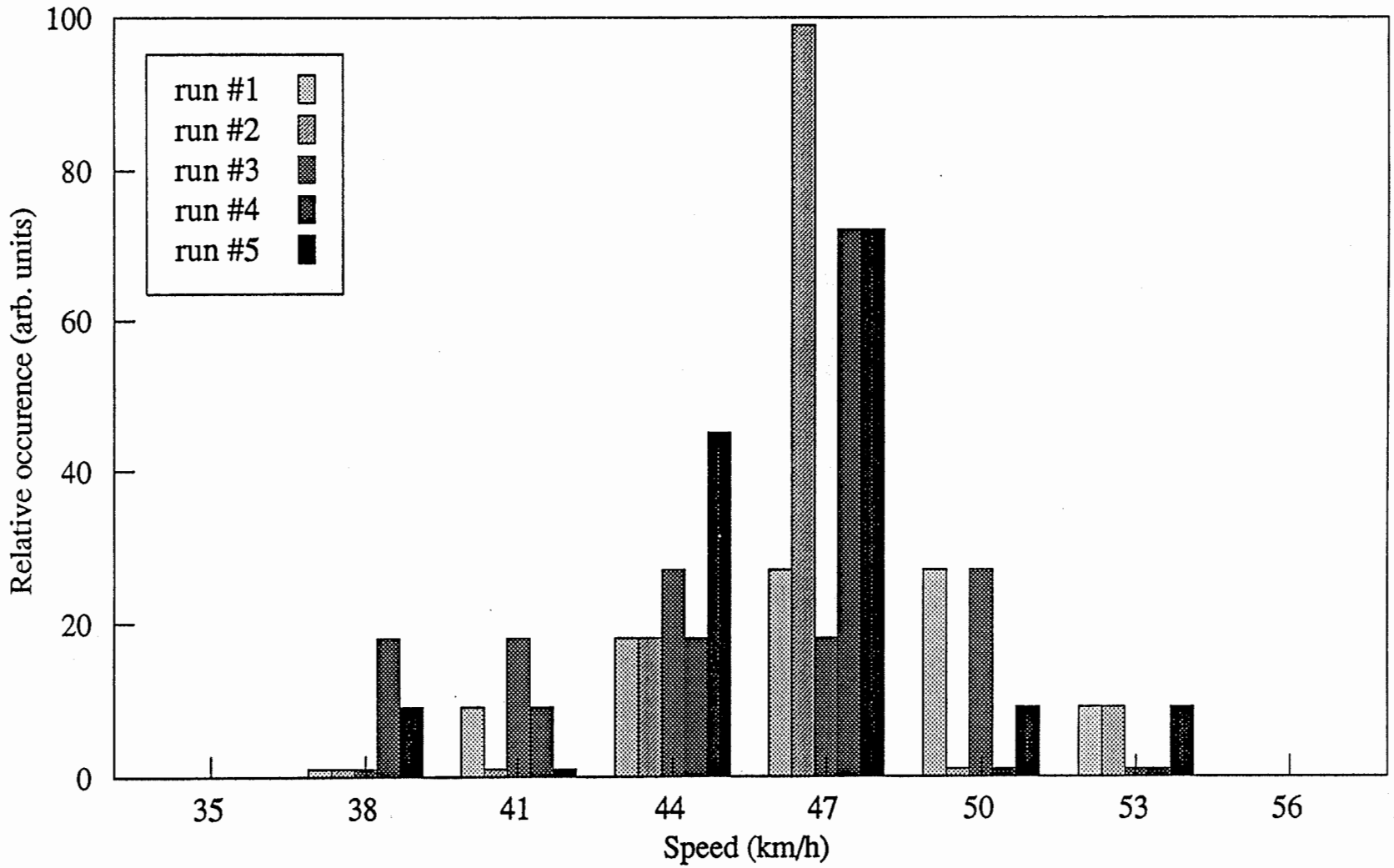

Figure 7.2 Speed distribution for selected runs (the nominal speed was 50 km/h).

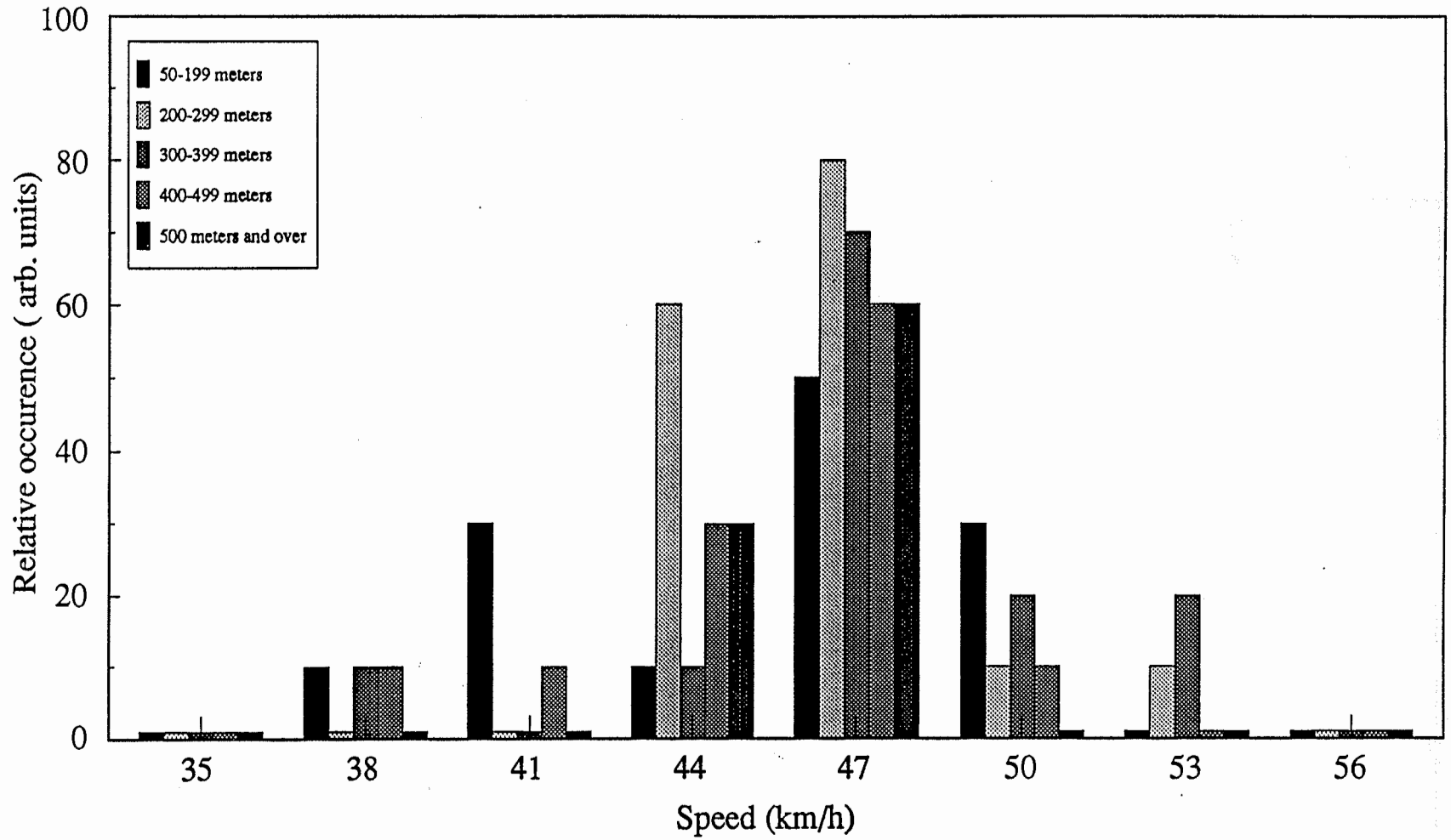

Figure 7.3 Distribution of speed values according to range (the nominal speed was 50 km/h).

according to equation 5.2, the smallest time jitter attainable was

$$\sigma_\delta = \left(\frac{1.8\,X\,10^{-11} \cdot 100\,X\,10^{-9}}{(0.07)^2 \cdot 100} \right)^{1/2} = 1.9 ns\ rms\ ,$$

and, from equation 5.3, the speed standard deviation, would have become

$$\sigma_v = \frac{\sigma_\delta \cdot c}{T} = \frac{1.9\,X\,10^{-9} \cdot 3\,X\,10^{8}}{1} = 0.57 m/s = 2.1 kmh^{-1}$$

about 1.6 times lower than the achieved accuracy. A certain number of reasons can be invoked to account for this discrepancy between the theoretical and achieved precision. First, the equation used to evaluate the time jitter was derived assuming that the pulses had small rise-time compared to their widths. Obviously, this isn't the case, the pulses emitted by the laser diode having a more triangular rather than trapezoidal shape. Secondly, the equation used is part of a larger set where each equation is used for a particular range of SNR's. Unfortunately, the SNR levels are nearby the boundary of validity for the equation used (the other equation would lead to even worse results). Once again then, a part of the discrepancy may be explained by that limit case. Finally, the number of samples was never 100 as was always assumed. Our tests rather showed that the number of pulses actually echoed rarely exceeded 90. (Actually, all the pulses emitted were reflected but the triggering/laser diode assembly sometimes missed a beat.)

It is our belief that the 1.6 factor between the theoretical and experimental results is small enough to demonstrate that the measurements taken are in pretty good agreement with the theory. We therefore conclude, that the feasibility of a time of flight radar has been demonstrated, provided that the improvements suggested in the next chapter are taken into account.

8. IMPROVEMENTS.

While promising, the results presented in the last section nevertheless show that the actual design requires some improvements.

The first major improvement (which is the most significant and paradoxically one of the easiest to achieve) concerns the replacement of the laser pulser. As we have noted earlier, the pulser used in our experiments had a 200 ns pulse width with a 100 ns rise-time. The replacement of this pulser by a faster model (e.g. 10 ns rise-time with 30-40 ns pulsewidth) would be beneficial from two standpoints. First, the reduction in the pulse width would permit the use of higher peak power pulses resulting, in higher SNR's and therefore in a better resolution. Secondly, a shorter rise-time would also lead to better resolution as can be seen from equation 5.2.

The background (sky) noise reduction is the second major improvement. In the feasibility study, it was predicted that the background noise (which is proportional to the detector field-of-view) could be neglected. However, the detector field-of-view (FOV) then assumed was much lower than what was achieved in practice. Therefore, a reduction in the field-of-view would result in a sensible reduction of the background noise. This reduction of the FOV implies some rework of the optical design, anyway required for size and costs reductions purposes.

As a third improvement, an increase in the number of pulses averaged could also be considered. There is however an upper limit to the number of pulses that can be sent dictated by the pulser and laser diode maximum repetition rates. In parallel with the increase in the number of pulses, a more efficient signal processing scheme could be devised. For example, the use of a linear regression algorithm instead of plain averaging might yield an appreciable gain in accuracy.

Aside from these accuracy-driven improvements, other aspects of the design deserve a second look. First, it appears mandatory that the acquisition time be reduced below the 1s barrier. We believe there is an upper limit to the acquisition time set by two practical limits. While it is true that the device do not need to remain very thightly aimed toward the target during the measurement, the acquisition time should certainly remain below 0.5 s (and most probably around 0.3 s) to prevent the readings from being affected by unvoluntary movements. Secondly, the acquisition time is also upper-bounded by a marketing reason: the system response time must be kept low for the user to feel comfortable, that is, the psychological impact (confidence, ease of use) of a long response time should not be underestimated. Unfortunately, the decrease in response time and the increase in accuracy are incompatible as can be readily understood by inspection of equation 5.3. Thus, the acquisition is also lower bounded as a result of the trade-off between the system response time and its accuracy.

There is a third area where the actual radar electronics design could be improved. In essence, the system designed and built fulfills all the requirements. However, most of the system is actually built out of ECL logic building blocks, a costly and power hungry technology used mainly because of the high clock speeds involved. It is therefore our opinion that proper use of an ECL prescaler coupled to lower speed TTL devices might permit a reduction in both production costs and power consumption. In addition, the board size and component count could be lowered by replacing the "glue chips" by a programmable gate array. These changes would result in a smaller, cheaper and less power consuming board. The performances should however remain unaffected by these changes. Lastly, with the same space and costs savings considerations in mind, it would be advantageous to replace the current PLL oscillator by a commercially available clock.

9. FUTURE OVERVIEWS.

This section will summarize the main results and propose designs and processing circuits suited for an industrial laser traffic radar prototype. Once again, the section will be divided into two parts: the optical set-up and the signal processing circuit.

9.1 PROPOSALS FOR THE OPTICAL SET-UP.

Before presenting two different designs we will recall the main conclusions of the optical field tests. They are as follow:

1- the signal level decreases at best as $R^{-3.25}$ and at worst as $R^{-3.8}$ (see figure 4.2),

2- to ease the tracking, we need an aiming system,

3- with about 25 W peak power, we obtained a maximum range of 700 m for an incoming car and a range of 1.2 km for a receding one,

4- a laser line filter decreases the noise by a four-fold time while the received signal level is decreased to half (this decrease could be reduced by proper coating design).

We also know that the industrial traffic radar prototype must be hand-hold, light weight and eye-safe. For this last requirement, we know that the largest emitting surface gives the safest apparatus for a given pulse energy and pulse shape. To produce a light weight apparatus, Fresnel lenses are best suited since they are thin plastic plates (about 2 mm thickness) with grooves on to produce the lens effect. Fortunately, they are also the cheapest lenses available on the market especially when a diameter greater than 5.1 cm (2 inches) is required. Moreover, on the receiver side of the radar prototype, a Fresnel lens gave the best results. On the emitter side, a set of

many Fresnel lenses could probably give as good results as it was obtained during the field tests with a collimator and cylindrical lenses.

The aiming system will also need to be more precise and particularly more stable as the laser beam divergence will be decreased. On the other hand, the return signal level was shown to be higher at a fixed range and to decrease more slowly with the range when the beam divergence was smaller. The best case was an $R^{-3.25}$ signal decrease with range (see figure 4.2 for details). We must also remember that a 100 km/h moving car travels 27.8 m in 1 s and then the laser radar user will, in most cases, have to track the car even if the measure lasts for less than 0.5 s.

Knowing the above characteristics and requirements, two different designs for a hand-hold laser traffic radar could be produced. One is a gun-like radar and the other, a binocular-like apparatus. Figure 9.1 presents the gun design and figure 9.2, the binocular one.

The hand-hold gun radar presented on figure 9.1 uses only one lens to emit and receive the light from the target. Some active or passive element inside the apparatus must then be used in order to send the received light onto the photodetector instead of back onto the laser diode. To do so, a polarizing beam splitter or a polarizing beamsplitter together with a $\lambda/4$ waveplate can be used. With a polarizer only, some power is lost at the emission and at the reception. With the polarizer or cubic polarizing beamsplitter (see figure 9.1) in combination with a $\lambda/4$ waveplate, no loss will theoretically be seen when light undergoes only one reflection before coming back. However, light reflected on headlights or on retroreflectors is more likely to undergo more than one reflection before coming back. Then, a detailed field test study has to be conducted to really analyze the polarization content of the return signal from a car.

Up to now, only preliminary tests on the polarization of the return signal have been conducted on separate car parts. The main results are presented in table 9.1. In this table, only the percentage of polarization of the return signal is given but it has been observed that the plane of polarization changed when the light underwent more than one reflection before coming back.

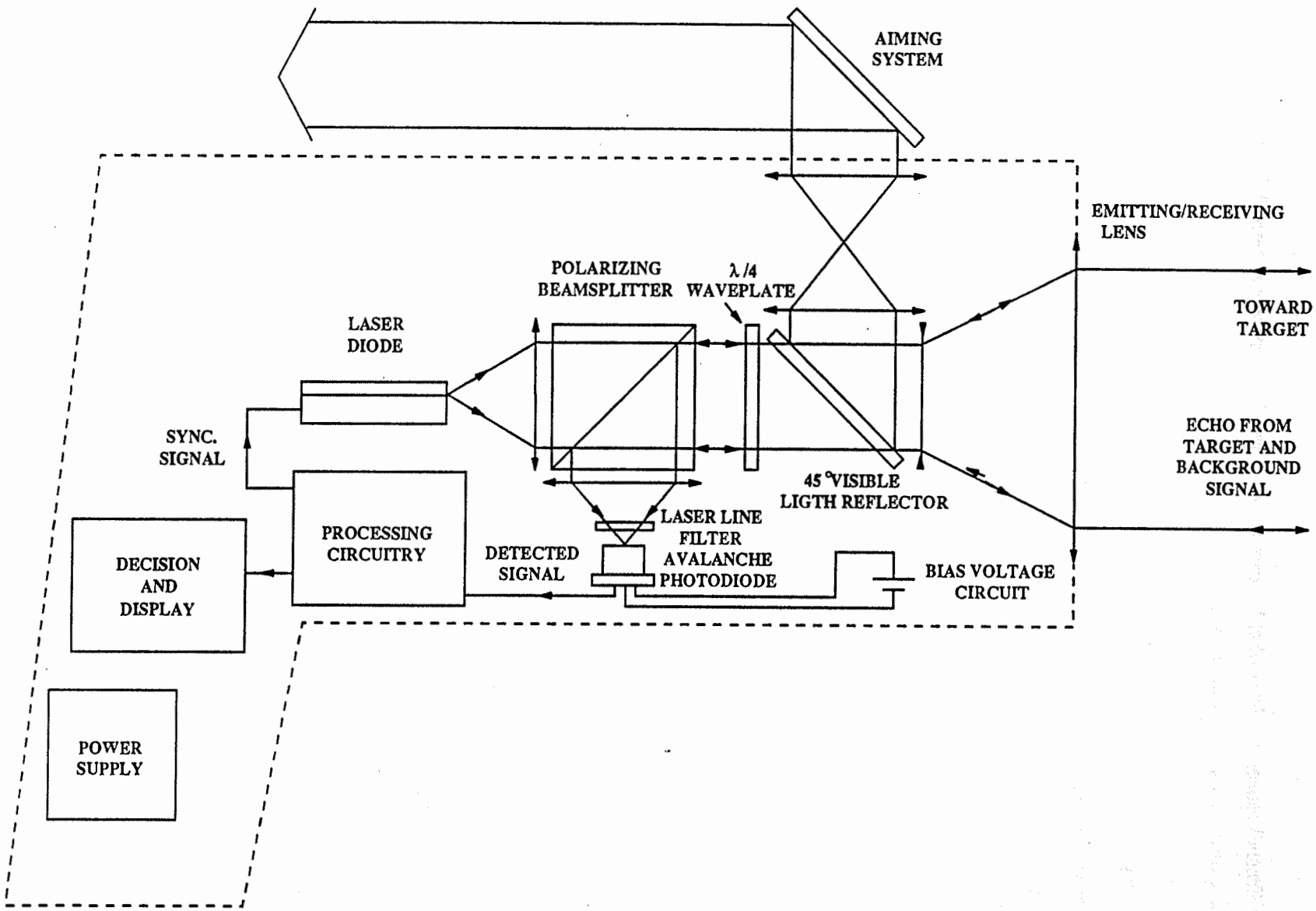

Figure 9.1 Gun-like laser traffic radar proposal.

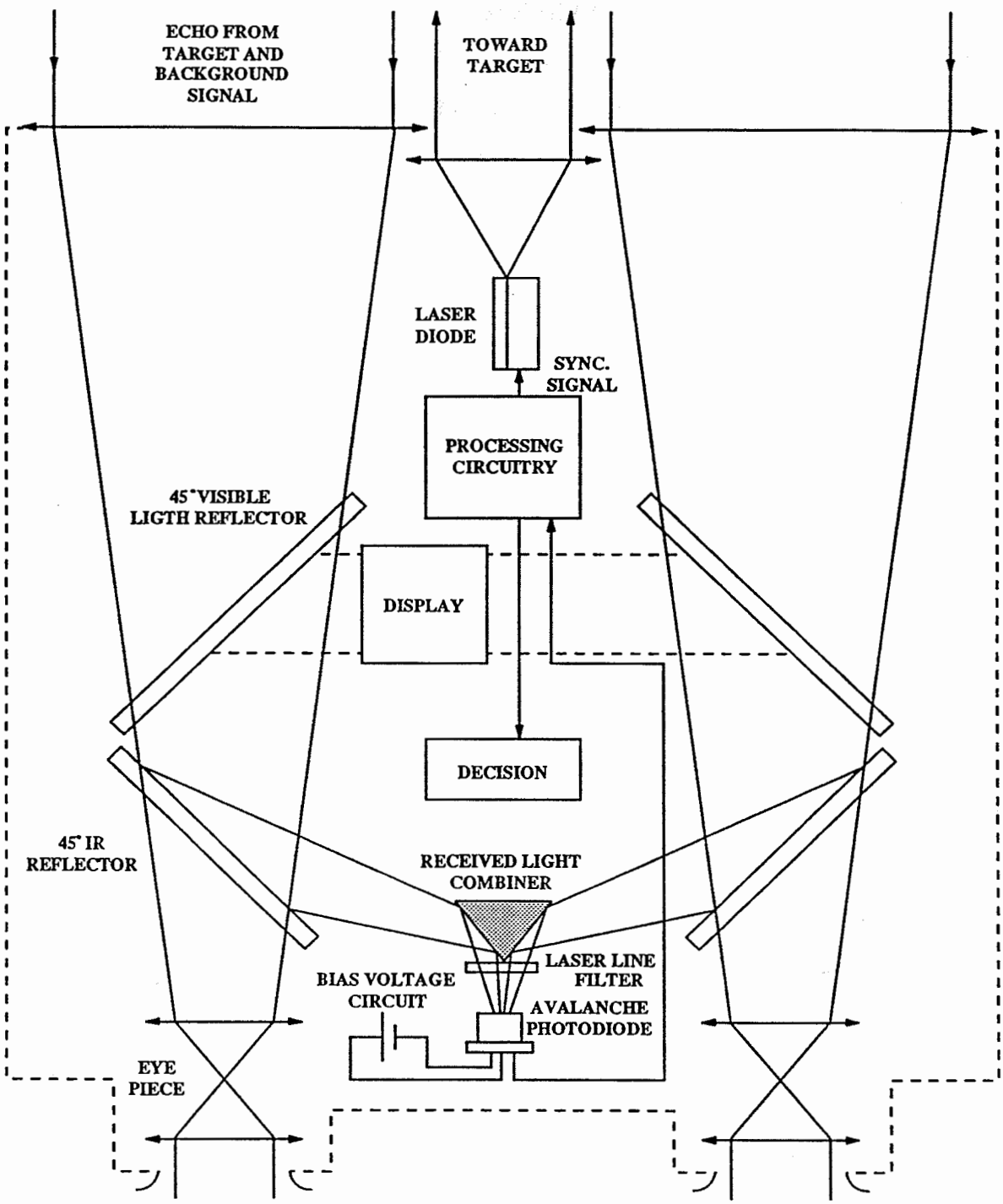

- OTHER POSSIBILITIES
  - ONE SIDE USED FOR EMISSION AND THE OTHER FOR DETECTION
  - BOTH SIDE USED FOR EMISSION AND DETECTION WORKING WITH LASER DIODE NATURAL POLARIZATION

Figure 9.2 Binocular laser traffic radar proposal.

TABLE 9.1

Polarization characteristics of the return signal from different parts of a car (Preliminary results)

	White paint	Headlight	Retroreflector
Specular Reflection $P_{\perp}/P_{\parallel}$	97,5 %	95,5 %	63,5 %
Diffuse Reflection $P_{\perp}/P_{\parallel}$	67 %	Unpolarized	--

As a matter of fact, the polarization angle difference between the specular reflections of white paint (one reflection) and headlight (at least two reflections) was around 60%. With a detailed field test study, we will see how the $\lambda/4$ waveplate will work with light reflected from a car. It is possible that only a polarizer gives better results than the polarizer-$\lambda/4$ waveplate combination and, at a lower cost.

Figure 9.1 also shows the aiming system of the gun radar which is mounted on its the case. The aiming system also uses the emitting/receiving lens. The visible light is, in that case, brought to the operator by the use of a 45° visible light reflector which reflects light only in the 400-700 nm wavelength range and transmits the IR light like the 860 nm laser output.

The way the laser gun is operated is exactly the same as a real gun; the apparatus is held with one or both hands with the arm(s) extended. From a stability point of view, the apparatus

could require more physical skills than the binocular design. Also, the apparatus would really look like the actual microwave traffic radar.

On the other hand, the binocular set-up really brings a new way to use a traffic radar. This kind of apparatus looks more passive than the radar gun. The bioncular set-up is also more versatile. The apparatus could be designed exactly like the set-up of figure 9.2 with one lens to emit and two lenses to receive the signal. Another possibility is to use only two lenses; in that case, one side of the binocular could be designed to emit and the other to receive the laser light. The binocular could also be made with only one output lens. In that case, it would work with the polarization of light exactly like the gun radar of figure 9.1. As a matter of fact, in that last configuration only the aiming system would have to be changed from the gun-like set-up.

On a stability point of view we think that the binocular set-up would require less physical skills to be used than the gun set-up since it would be held on the forehead.

If we come back to figure 9.2, we see that the proposed configuration would need a received light combiner. This optical piece could be difficult to align in order to send all the received light onto the detector. If this is found to be the case, binocular with only two lenses or one lens would be more advantageous to develop.

The final design will need to be chosen to cover a certain range. The shorter the range will be, the larger the number of possible designs will be. The logic behind that is very simple. To increase the range of the radar, one can increase the emitted power or the surface of the focussing lens (see figure 3.1). Since we are always limited by the eye-safety rules, which limit the emitted energy per unit area, an increase in the emitted power also means a surface increase of the laser light collimating system. Then the emitter and maybe the receiver surfaces will increase with the range. At first sight, for a range greater than 500 m using the signal processing unit, a one lens system would greatly help to produce a compact system. It is possible to produce both designs, gun and binocular, in that configuration. Moreover, it will always be possible to produce a more eye-safe design with a one lens system at a fixed range. However,

more analysis and field tests on polarization of the return light are needed to propose a final design using only one lens since some polarization modifications could occur due to the reflection on a car.

The final design will also have to take into account the marketing aspect. We believe that this marketing aspect will need to be discussed with the eventual producer and distributor of the apparatus.

We have already seen in section 8 that the electronics design was rather close to its final form. It was also shown that a few modifications to some parts of the actual design would greatly improve on the performances acheived with the laboratory model.

In addition, we saw that a reduction in cost, size and power consumption were probably the most challenging goals that remain to be acheived. A number of improvements have been suggested to fulfill these requirements. For example, a change from ECL to TTL technology, the use of surface-mount components and even an application specific IC (ASIC or custom chip) are among the solutions applicable.

The problem of the high voltage (300-400 V) required by the detector can be solved with commonly available small footprint (a few square inches) high voltage supplies. The whole circuitry could be operated off a 12 V standard car battery or from a separate battery pack. Some regulating devices would however still be needed to provide the circuits with standard operating voltages. Finally, a special care would have to be given to electromagnetic shielding, both to prevent cross-talk between different circuit area and to meet state and federal regulations (FCC, etc...).

10. CONCLUSION.

We have demonstrated the feasibility of laser based traffic radar. The technique used was the time of flight and the power used with the collimating lens surface was eye-safe.

With that technique and a 25 W peak power pulse, a maximum range of 700 m for an incoming car was observed. For a receding car, a range of more than 1.2 km was observed. When using the complete system comprising the data processing unit, these ranges were respectively decreased to 400 m and 600 m.

The most appropriate parts to aim at were found to be the headlight for an incoming car (there was no front licenses on cars used for the field trials) and the parking lights comprising corner cube elements for a receding car. Weather conditions were also found to influence the maximum range at which we can measure the speed of a car. However, further investigation are required to really establish the limit of the technique under special conditions like rain or snow.

An analysis of the polarization characteristics of the received light under many conditions especially for many kinds of cars (model and color) is believed to greatly help choosing the final apparatus design, while the marketing aspect of one or the other design will have to be evaluated by the producer or distributor of the laser traffic radar.

The electronic processing scheme proved to be efficient. A few modifications would greatly improve the performances. Most of the work that remain to be done in this area concerns miniaturization and power consumption reductions.

11. REFERENCES.

1. Taillon, Y. and Morin A., "Feasibility Study of a Laser Traffic Radar", National Optics Institute, April 1991.

2. Boynton, R. (1974)., "Handbook of Perception", E.C. Carterette and M.P. Friedman, eds., Vol. 1. Copyright 1974 Academic Press.

3. Committee on Colorimetry Optical Society of America, "The Science of Color", by Edwards brothers Inc., Ann Arbor, Mich. 1973.

APPENDIX A

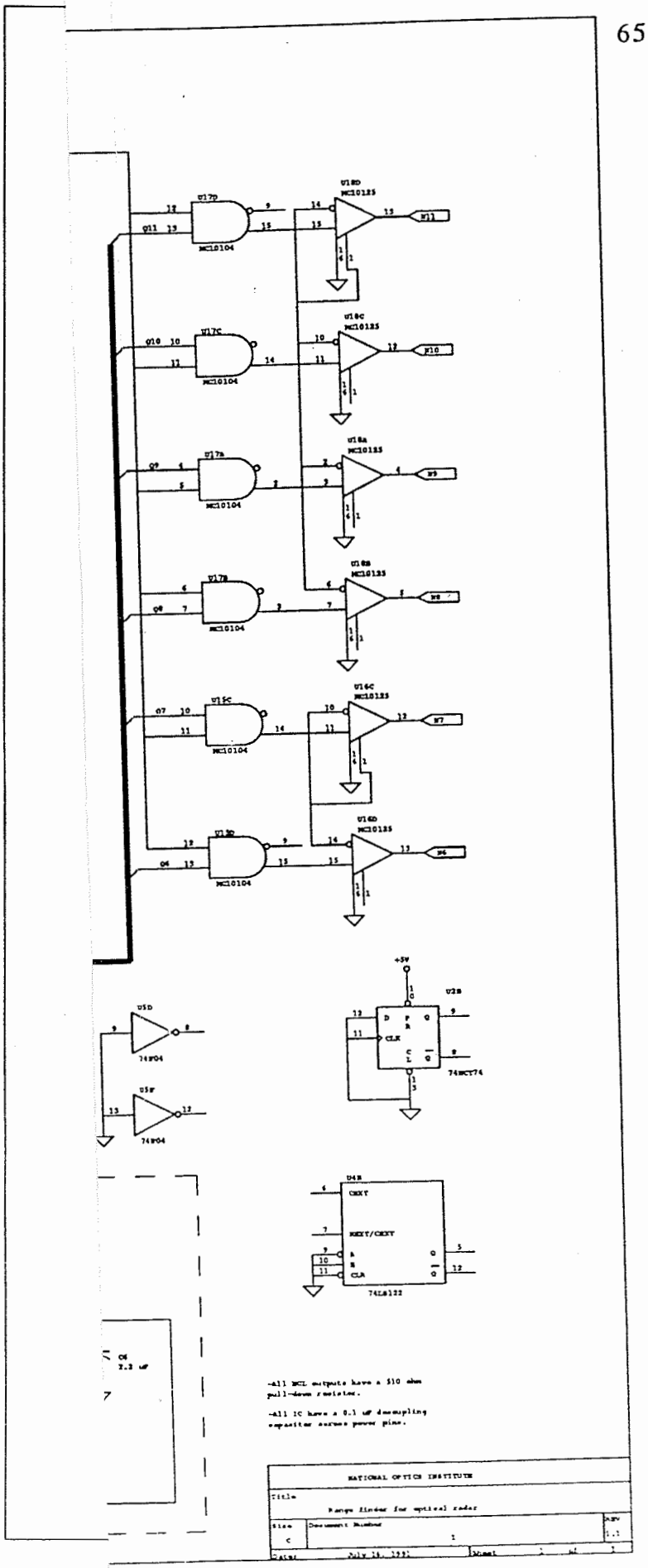
U18D MC10125
U17D
MC10104
Q11
M11
U18C MC10125
U17C
MC10104
Q10
M10
U18A MC10125
U17A
MC10104
Q9
M9
U18B MC10125
U17B
MC10104
Q8
M8
U16C MC10125
U15C
MC10104
Q7
M7
U16D MC10125
U15D
MC10104
Q6
M6
U5D
74F04
U5F
74F04
+5V
U2B
74HCT74
U4B
CEXT
REXT/CEXT
CLR
74LS122
-all ECL outputs have a 510 ohm pull-down resistor.
-all IC have a 0.1 uF decoupling capacitor across power pins.
NATIONAL OPTICS INSTITUTE
Title
Range finder for optical radar
Size
C
Document Number
1
REV
1.1
Date: July 14, 1991
Sheet 1 of 1

APPENDIX B

```
/****************************** RADAR COUNTER ******************************
*
*       Evaluates the range and speed of a vehiclae by a time of flight method
*
*
*   written by :    Andre Morin, Sylvain Lord
*   date       :    06/08/91
*   modified   :    07/15/91
*/


/************************* PREPROCESSOR INSTRUCTIONS ********************/

#include   <conio.h>
#include   <dos.h>
#include   <graphics.h>
#include   <math.h>
#include   <stdio.h>
#include   <stdlib.h>
#include   <string.h>
#include   <time.h>

#define    data_board_ctrl   0x303
#define    portA             0x300
#define    portC             0x302
#define    bitC7_high        0x80
#define    Light_Speed       3.0E+8          /* vitesse de la lumiere */
#define    Clk_Period        5.21E-9         /* 1 / 192MHz  =  5.21 ns */
#define    ESC               0x1B            /* escape = ascii 27 en hexadecimal */
#define    Const_Prop        Light_Speed*Clk_Period/2


/****************************** FUNCTIONS PROTOTYPES **********************/

char   *cvtfl_str (float, int);
float  avg_dist (int indx);

/********************************** DEFINITIONS ***************************/

float  radar_value;
char   vitesse[30], distance[30];
float  radar_vector[2][100];

/*****************************************************************************
*  MAIN      initialisation and range and                                    *
*            speed calculations                                              *
*****************************************************************************/

void main( void )
    {
        int  g_driver, g_mode;
```

```
int nb_pts1, nb_pts2, indx3;
long   indx1;
float  first_range, second_range, speed, avg_range;
float  Acq_Time = 1.0, Syst_Err=25.5;

/* drawing of main screen */
detectgraph(&g_driver, &g_mode);
initgraph(&g_driver, &g_mode, " ");
setbkcolor(BLUE);
setcolor(YELLOW);
settextstyle(3, 0, 0);
setusercharsize(1, 2, 1, 2);
outtextxy(200, 15, " LASER TRAFFIC RADAR ");
outtextxy(163, 35, " (c) National Optics Institute 1991");
outtextxy( 260, 408, " INFO ");
outtextxy(75, 450, " Strike any key to start acquisition or press 'ESC' to quit");
rectangle(0, 0, 639, 479);
rectangle(3, 3, 635, 57);
line(265, 415, 3, 415), moveto(3, 415);
lineto(3, 60), lineto(635, 60), lineto(635, 415), lineto(300, 415);
line(265, 418, 3, 418), moveto(3, 418);
lineto(3, 476), lineto(635, 476), lineto(635, 418), lineto(300, 418);
setusercharsize(2, 2, 2, 2);
outtextxy(100, 200, " SPEED: "), outtextxy(325, 200, " km/h ");
outtextxy(95, 240, " RANGE: "), outtextxy(325, 240, " meters ");
setviewport(210, 190, 325, 350, 1);
outportb( data_board_ctrl, 0x93);
while(getch() != ESC)                    /* program terminates on ESC */
{
    clearviewport();
    first_range=avg_dist(0);
    for(indx1=0; indx1<170640L; ++indx1);/* timer waits for one second */
    second_range=avg_dist(1);
    radar_value=0.0;
    nb_pts1=0;
    for(indx3=0;indx3<100;indx3++)
    {                                    /* remove impossible values of first burst */
        if ((radar_vector[0][indx3] < 1.1 * first_range)&
            (radar_vector[0][indx3] > 0.9*first_range))
        {
            nb_pts1++;
            radar_value+=radar_vector[0][indx3];
        }
    }
    if (nb_pts1 > 0)
    {
        first_range=radar_value/nb_pts1;
    }
    radar_value=0.0;                     /* process second burst */
    nb_pts2=0;
    for(indx3=0;indx3<100;indx3++)
    {
```

```
            if ((radar_vector[1][indx3]<1.1*second_range)&
                (radar_vector[1][indx3]>0.9*second_range))
            {
                nb_pts2++;
                radar_value+=radar_vector[1][indx3];
            }
        }
        if (nb_pts2 > 0)
        {
            second_range=radar_value/nb_pts2;
        }
        if ((nb_pts1 > 0) & (nb_pts2 > 0))          /* calc of speed and range */
        {
            speed=(second_range-first_range)*Const_Prop/Acq_Time*3.6;
            avg_range=(first_range+second_range)*Const_Prop/2-Syst_Err;
        }
        else
        {
            speed=0.0;
            avg_range=0.0;
        }
        strcpy (vitesse,  itoa ((int)speed, vitesse,  10));
        strcpy(distance, itoa ((int)avg_range, distance, 10));
        (speed > -1.0) ? outtextxy(35, 10, vitesse) : outtextxy(15, 10, vitesse);
        outtextxy(35, 50, distance);
    }
    closegraph();
}

/*****************************************************************************
*  AVG_DIST   calculates distance                                            *
*             by averaging over one hundred values                           *
*****************************************************************************/

float avg_dist(int indx)
{
    int indx1, indx2 = 0;
    float   radar_value  = 0.0;


    for(indx1=0; indx1<100; ++indx1)
    {
        outportb (portC, bitC7_high);           /* toggle pulse emit bit */
        outportb (portC, 0);
        radar_vector[indx][indx1]=(float)inport(portA); /* read value */
        if (radar_vector[indx][indx1] != 0.0)
        {
            ++indx2;
            radar_value+=radar_vector[indx][indx1];
        }
    }
```

```
    return((indx2==0)?(0.0):(radar_value/indx2));
}

/*****************************************************************************
*  CVTFL_STR()   Converts floating point number                              *
*                to a character chain                                        *
*****************************************************************************/

char    *cvtfl_str (float nombre, int ndec)
{
    char    buf1[10], buf2[30];
    double entier, fraction, valeur=0.0;
    int     x;

    fraction=modf (nombre, &entier);
    if (((int)entier == 0) && (nombre < 0))
    {
        strcpy (buf2, "-0");
    }
    else
    {
        ltoa ((long)entier, buf2, 10);
    }
    strcat (buf2, ".");
    for (x=0; x<ndec; x++)
    {
        fraction=fabs (10.0*fraction-valeur);
        valeur=10.0*floor (fraction);
        strcat (buf2, itoa ((int)fraction, buf1, 10));
    }
    return (buf2);
}
```